

1 **Compartmentalization of mRNAs in the giant,** 2 **unicellular green algae *Acetabularia acetabulum***

3

4 ***Authors***

5 Ina J. Andresen¹, Russell J. S. Orr², Kamran Shalchian-Tabrizi³, Jon Bråte^{1*}

6

7 ***Address***

8 1: Section for Genetics and Evolutionary Biology, Department of Biosciences, University of
9 Oslo, Kristine Bonnevis Hus, Blindernveien 31, 0316 Oslo, Norway.

10 2: Natural History Museum, University of Oslo, Oslo, Norway

11 3: Centre for Epigenetics, Development and Evolution, Department of Biosciences, University
12 of Oslo, Kristine Bonnevis Hus, Blindernveien 31, 0316 Oslo, Norway.

13

14 ****Corresponding author***

15 Jon Bråte, jon.bråte@ibv.uio.no

16

17 ***Keywords***

18 *Acetabularia acetabulum*, Dasycladales, UMI, STL, compartmentalization, single-cell, mRNA.

19

20 **Abstract**

21 *Acetabularia acetabulum* is a single-celled green alga previously used as a model species for
22 studying the role of the nucleus in cell development and morphogenesis. The highly elongated
23 cell, which stretches several centimeters, harbors a single nucleus located in the basal end.
24 Although *A. acetabulum* historically has been an important model in cell biology, almost
25 nothing is known about its gene content, or how gene products are distributed in the cell. To
26 study the composition and distribution of mRNAs in *A. acetabulum*, we have used quantitative
27 RNA-seq to sequence the mRNA content of four sections of adult *A. acetabulum* cells. We
28 found that although mRNAs are present throughout the cell, there are large pools of distinct
29 mRNAs localized to the different subcellular sections. Conversely, we also find that gene
30 transcripts related to intracellular transport are evenly distributed throughout the cell. This
31 distribution hints at post-transcriptional regulation and selective transport of mRNAs as
32 mechanisms to achieve mRNA localization in *A. acetabulum*.

33 Introduction

34 Large and complex morphological forms are predominantly found among multicellular
35 organisms such as animals, plants and kelps. However, also several single celled organisms
36 have elaborate cellular morphologies, and it has therefore been previously argued that
37 multicellularity is not a requirement for the formation of structural complexity (Kaplan, 1992;
38 Kaplan et al., 1991; Niklas et al., 2013; Ranjan et al., 2015). By subcellular
39 compartmentalization of RNA or proteins, single-celled organisms can chamber their bodies
40 into differently shaped subunits, further facilitating development of sophisticated body plans
41 without cellularization (Kaplan, 1992; Kaplan et al., 1991; Niklas et al., 2013). The green algae
42 order Dasycladales harbors multiple examples of single-celled species with highly elaborate
43 and complex cellular morphologies. With only a single nucleus, these algae have evolved into
44 numerous morphological forms, and can grow up to 20 cm long (Berger, 1990, 2006).

45
46 Being used as a model organism to study the link between genetics and cellular development,
47 *Acetabularia acetabulum* is the most studied dasycladalean species. This alga is a tropical,
48 marine species found in shallow waters in the Mediterranean Sea, Northern Africa and South-
49 West Asia. Divers often refer to *A. acetabulum* as “mermaids wineglass” because of its
50 distinctive morphology; the basal rhizoid, which hosts the nucleus as well as ensuring anchoring
51 of the cell to a substrate, is followed by a naked, elongated stalk with a slightly concave and
52 disc-looking structure (cap), at the apical end (Figure 1A).

53
54 Through his ground breaking amputation and grafting experiments, Joachim Hämmerling was
55 the first to identify the presence of substances controlling the subcellular morphogenesis of *A.*
56 *acetabulum* (Hämmerling, 1934a, 1934b; Hämmerling, 1953). He also showed that these
57 substances were distributed in gradients, with the highest accumulation at the cap and rhizoid
58 regions (Hämmerling, 1934c; Hämmerling, 1963). These morphogenetic substances were later
59 shown to consist of mRNA (Baltus et al., 1968; Garcia et al., 1986; Kloppstech, 1977; Naumova
60 et al., 1976), but the content of the RNA gradient, and whether it was composed of
61 homogeneously or differentially distributed RNA transcripts was not known.

62
63 A few studies have tried to decipher the RNA gradient in *A. acetabulum*. Naumova et al. (1976)
64 argued that the gradient was due to differential metabolism of chloroplast ribosomal RNA along
65 the cell rather than differential transportation of nuclear mRNA. A more recent study by Vogel

66 et al. (2002) examined the expression of 13 house-keeping genes and found differential
67 accumulation of several gene transcripts, where some transcripts seemed to accumulate in the
68 rhizoid, some in the cap, while others were evenly distributed along the cellular body. Serikawa
69 et al. (1999) demonstrated that the *A. acetabulum*-specific homeobox-containing gene,
70 *Aaknox1*, shifted localization from being evenly distributed during vegetative growth, to basal
71 accumulation in the final stages of the *A. acetabulum* life cycle. And both the transcripts
72 encoding carbonic anhydrases as well as their translated protein products were shown to be co-
73 localized in the apical parts of adult *A. acetabulum* cells (Serikawa et al., 2001), indicating that
74 localization of mRNA is a mechanism for correct localization of protein. Altogether, these
75 studies suggested that subcellular localization of mRNA is common in the *A. acetabulum* cell,
76 and an important mechanism for establishment of subcellular structures.

77
78 mRNA localization has also been demonstrated in another gigantic single-celled green algal
79 genus, *Caulerpa* (Arimoto et al., 2019; Ranjan et al., 2015). These single-celled organisms
80 contain hundreds of nuclei distributed across the cell and the localization of mRNA is achieved,
81 at least in part, by differential nuclear transcriptional regulation in the different parts of the cell
82 (Arimoto et al., 2019). Unlike *Caulerpa*, *A. acetabulum* has only a single nucleus (located in
83 the basal rhizoid) and clearly the mechanisms behind the subcellular localization of mRNAs,
84 and ultimately the establishment of the cellular body plan, must be different. Although these
85 mechanisms are unknown, there are several indications that mRNAs are actively transported
86 along the cytoskeleton in *A. acetabulum*. Kloppstech et al., (1975a and 1975b) showed that
87 ribosomal- and polyadenylated RNA travel with different speeds in *A. acetabulum*, and that
88 polyadenylated RNA moved with a speed of 0.2 $\mu\text{m/s}$, which is much faster than movement
89 with normal diffusion, suggesting that RNA transportation is both active and specific. Further,
90 staining experiments performed on *A. peniculus* showed that actin proteins and polyadenylated
91 RNAs were co-localized, and that treatment with cytochalasin D (inhibitor of actin
92 polymerization) lead to a disruption of already established mRNA gradients (Mine et al., 2001).
93 These findings supported the theory that the cytoskeleton is involved in polar transportation of
94 mRNAs in *Acetabularia* species (Vogel et al., 2002).

95
96 The studies on the expression and localization of mRNAs in *A. acetabulum* has so far only been
97 performed on a restricted number of genes, and it is not known how general this phenomenon
98 is, and how gene localization is related to the observed gradients of RNA along the cell. We
99 have therefore in this study characterized the expression profile of all mRNAs in adult *A.*

100 *acetabulum* cells. To achieve this, we have exploited recent developments in single-cell RNA-
101 seq technology which allowed us to quantitatively sequence mRNAs from four subcellular
102 sections of the cell, the upper and lower parts of the stalk, and the rhizoid (Figure 1A). We
103 investigate whether subcellular compartmentalization is a general phenomenon for all types of
104 mRNAs in *A. acetabulum*, and whether the distribution of mRNAs can be coupled to the
105 formation of body plan and the complex cellular morphology of this algae.

106
107

108 **Methods**

109

110 **Culturing *Acetabularia acetabulum* cells**

111 *A. acetabulum* cells were cultured in cell/tissue culture flasks in Dasycladales Seawater
112 Medium prepared after the recipe of UTEX Culture Collection of Algae at The University of
113 Texas at Austin ([https://utex.org/products/dasycladales-seawater-
114 medium?variant=30991770976346](https://utex.org/products/dasycladales-seawater-medium?variant=30991770976346)). The medium was changed biweekly, and the algae were
115 kept in incubators with a 12/12h light/dark cycle (light intensity of 2500 lux) with a constant
116 temperature of 20°C.

117

118 **Dissection of cells and RNA isolation**

119 The *A. acetabulum* cells were 5-8 cm long with fully grown caps, but no apparent gametes in
120 the gametangia, and no whorls along the stalk (Figure 1A). The cells were washed three times
121 in 1X PBS to remove residues from the medium, and dissected into four subcellular regions;
122 the “cap” (incision about 2 mm from the apical tip or just below the cap), “rhizoid” (incision
123 about 2 mm above the rhizoid), “upper stalk” (the upper half of the stalk) and “lower stalk” (the
124 lower half of the stalk). Dissection was carried out in dry petri dishes to limit cytoplasmic loss,
125 and new, sterile scalpels were used between incision. Subcellular regions from 5 – 8 adult cells
126 were pooled together to achieve sufficient RNA quantities. The procedure was repeated to
127 create seven replicates of RNA extraction. The subcellular samples are numbered according to
128 which batch of cells they originate from, e.g. the samples named “Cap 19” and “Rhizoid 19”
129 are the cap- and rhizoid sections from the same batch of individuals (batch19).

130

131 The dissected pieces were transferred to green MagNA Lyser Green Beads (Roche Life
132 Science, Germany), containing lysis buffer (see below), and flash frozen in liquid nitrogen.

133 RNA from 3 batches (batch 17, 19 and 25) was isolated using the “Single Cell RNA Purification
134 Kit” (NORGEN BIOTEK CORP, Canada) with an 8 ul elution buffer. RNA from the remaining
135 4 batches (batch 26, 27, 45 and 46) was isolated using the “Total RNA Purification Kit”
136 (NORGEN BIOTEK CORP, Canada) with 40 ul elution. RNA quality and quantity were
137 inspected on the Agilent 2100 Bioanalyzer using the Agilent RNA 6000 Pico kit (Agilent
138 Technologies, Inc, Germany).

139

140 **Library preparation and sequencing**

141 ERCC RNA Spike-In Mix I (ThermoFisher Scientific, Massachusetts, USA) was added to each
142 sample before mRNA enrichment. The amount of added ERCC Spike-In Mix was adjusted to
143 the amount of RNA in each sample, according to the manufacture’s protocol. mRNA
144 enrichment was performed using NEXTflex™ Poly(A) Beads (BIOO Scientific Corporation,
145 Texas, USA) before library preparation with the NEXTflex Rapid Directional qRNA-Seq
146 Library Prep kit for Illumina sequencing (BIOO Scientific Corporation, Texas, USA). This
147 library preparation kit assigns a unique molecular identifier (UMI), or Stochastic Label (STL),
148 to both ends of the mRNA fragments after enzymatic fragmentation, but before cDNA synthesis
149 and amplification. This allows for distinguishing between PCR duplicates and true identical
150 sequences which map to the same loci, ensuring a better quantitative representation of the
151 original number of mRNA fragments in the samples than standard RNA-seq library protocols
152 without UMI-labelling (Toloue et al., 2013). A total of 30 PCR cycles were run for sample
153 17.1-4, 25 cycles were run for sample 25.4 and 26.4, and 20 cycles were run for sample 19.1-
154 4, 25.1-3, 26.1-3, 27.1-4, 45.1-4 and 46.1-4 to create libraries of approximately equal quantities
155 as measured by gel electrophoresis.

156

157 The 28 libraries were sequenced on the Illumina HiSeq4000 platform producing 150 bp Paired-
158 End sequences (with an insert size of 350 bp). The sequencing was performed at the Norwegian
159 Sequencing Centre (www.sequencing.uio.no) at the University of Oslo.

160

161 ***De novo* transcriptome assembly and annotation**

162 In order to obtain a complete transcriptome representing as many transcripts as possible to use
163 for gene quantification, the resulting sequences from the 28 adult sequence libraries were
164 assembled together with 20 transcriptome sequence libraries from various developmental stages
165 of *A. acetabulum* (unpublished data generated by our research group). Briefly, the assembly

166 was performed by first removing the nine first UMI bases of each sequence (from the 5' end)
167 with Trimmomatic v/0.35 (Bolger et al., 2014). Further, the 3'-adaptor sequences, and low-
168 quality sequences (phred score < 20) were trimmed. Only sequences longer than 36 bp were
169 retained. An additional trimming with TrimGalore v/0.3.3
170 (http://www.bioinformatics.babraham.ac.uk/projects/trim_galore/) was performed to remove
171 any remaining adaptor sequences. ERCC RNA spike-ins were removed from the data set by
172 mapping the reads to the known ERCC RNA spike-in sequences using Bowtie 2 v/2.2.9
173 (Langmead et al., 2012). A total of 2,095,599,508 paired end reads (1,047,799,754 pairs) were
174 obtained after preprocessing and used for transcriptome assembly. *De novo* assembly was
175 performed using Trinity v/2.5.1 (Grabherr et al., 2011). To reduce the number of possible
176 mapping sites in downstream analysis, the transcriptome was reduced to the highest expressed
177 isoform for each gene. These isoforms were found by subsampling 10% of the sequenced reads
178 of every sample using the BMap package (Bushnell, 2015), mapping them to the trinity
179 assembly, and further extracting the isoforms with the highest coverage. Transcripts encoded
180 by the chloroplast- and mitochondrial genome were identified by Megablast against a
181 chloroplast database containing chloroplast genomes from 59 published green algae species,
182 and a database containing mitochondrial genomes from 24 published green algae species (Table
183 S1 and S2). Transcripts giving significant hits against the databases were further examined by
184 Megablast against the NCBI Nucleotide collection database in order to exclude possible
185 prokaryote contamination. Transcripts with no hits to either the plastid and mitochondrial
186 databases were considered as nuclear encoded. As mRNA enrichment with poly(A) beads does
187 not remove rRNA completely, rRNA transcripts were identified by Megablast against complete
188 or partial 18S, 28S and 5.8S sequences from 20 green algae species (Table S3).

189
190 Transcriptome completeness was assessed by BUSCO v3.0 (Simao et al., 2015) analysis against
191 the Chlorophyta and Eukaryote datasets. Since nuclear genes of *A. acetabulum* have an
192 alternative codon usage, where TGA is the only stop codon, and TAA and TAG instead encodes
193 glutamine (Jukes, 1996; Schneider et al., 1989), the alternative genetic code (translation table
194 6: Ciliate, Dasycladaen and Hexamita Nuclear Code) was used during BUSCO evaluation.

195
196 TransDecoder v/3.0.0 (Haas et al., 2013) was used to predict coding regions. Translation table
197 6 was used to translate nuclear encoded transcripts, translation table 16 (Chlorophycean
198 Mitochondrial Code) was used to translate mitochondrial encoded transcripts and translation
199 table 1 (Universal Code) was used to translate chloroplast encoded transcripts. Translation table

200 1 was also used for transcripts matching both the chloroplast and the mitochondrial database.
201 The minimum peptide length was set to 70 amino acids, and the single best ORF per transcript
202 Predicted peptide sequences were further annotated with the eggNOG-mapper v/5.0 (Huerta-
203 Cepas et al., 2017; Huerta-Cepas et al., 2019).

204

205 **Gene expression quantification, normalization and sample clustering**

206 In order to quantify the gene expression, processed reads (after removing UMI's and low quality
207 bases) were mapped to the transcriptome (the highest expressed isoform of each gene) with
208 Bowtie2 v/2.2.9 (Langmead et al., 2012) and gene count files were generated using dqRNASeq
209 (<https://github.com/e-hutchins/dqRNASeq>), a Unix script, developed for analyzing sequence
210 data obtained with the NEXTflex Rapid Directional qRNA-Seq Library Prep kit. By using the
211 resulting mapping file, together with the raw unprocessed reads, the script collapses paired
212 reads with identical start- and stop sites *and* identical UMIs (assumed PCR duplicates) and
213 count these as one, while fragments with identical start- and stop sites but different UMIs are
214 counted individually (these are assumed to originate from different RNA fragments).

215

216 The plotCountDepth function in the SCnorm R package (Bacher et al., 2017) was used to
217 calculate and visualize the relationship between sequencing depth and gene counts across
218 samples. For the highest expressed genes (i.e. carrying the most robust signal) there was a
219 positive relationship between sequencing depth and gene expression, and we therefore
220 continued with the normalization procedure in the DESeq2 package (Love et al., 2014). To
221 reduce the computational burden, we filtered the transcripts to have a minimum count of 1 (raw
222 count) in at least 4 samples before DESeq2 normalization (these would not have affected the
223 downstream statistical analysis as they would have been filtered out anyway).

224

225 To compare the similarity between samples based on the overall variation in transcript
226 abundance, the normalized counts were transformed using the variance stabilizing
227 transformation (VST) function in DESeq2 and the samples were clustered/visualized with PCA
228 plots using the ggplot2 package (Wickham, 2016).

229

230 **Differential transcript abundance estimation**

231 A Wald test (implemented in DESeq2), performed pairwise between the different subcellular
232 compartments, was used to identify transcripts with differential abundance between at least two

233 subcellular compartments. DESeq2 normalized read counts was used as input for the test. The
234 batch origin of each sample was added as a blocking factor in the test (added to the design
235 formula) to take into account any potential influence on the gene counts. Transcripts with
236 adjusted p-value < 0.05 were considered as significantly differentially abundant (DE). Only
237 nuclear encoded mRNAs were used in the DE test.

238

239 A Venn diagram was constructed using the systemPipeR package in R (Backman et al., 2016)
240 to visualize and compare the DE transcripts of each subcellular compartment. To visualize and
241 plot DE transcripts based on expression levels, the raw counts were converted to CPM's (count
242 per million) followed by TMM normalization (Trimmed Mean of M-values) using the edgeR
243 package in R (McCarthy et al., 2012; Robinson et al., 2010). The mean expression values were
244 further scaled and clustered in a heatmap using the Pheatmap package in R ([https://CRAN.R-](https://CRAN.R-project.org/package=pheatmap)
245 [project.org/package=pheatmap](https://CRAN.R-project.org/package=pheatmap)).

246

247 **GO-enrichment analysis**

248 GO-terms provided by EggNOG were converted to GO-slim with OmicsBox
249 (<https://www.biobam.com/omicsbox>), and GO-enrichment analysis on the differentially
250 distributed transcripts unique to the cap, upper stalk, lower stalk and rhizoid were performed
251 using the R package Goseq (Young et al., 2010). In addition, the stalk samples were analyzed
252 together by combining the uniquely differentially distributed transcripts from the upper- and
253 lower stalk samples, as well as the differentially distributed transcripts shared between them.
254 Lists of the unique transcripts from each subcellular compartment were extracted and inputted
255 into Goseq, together with a list of transcript lengths, to account for any bias introduced from
256 transcript length variation (longer transcripts might be easier to annotate or could receive more
257 GO-annotations than shorter transcripts). GO-terms with a false discovery rate (FDR) < 0.05
258 were considered enriched. The “hit percentage” of each enriched GO-term within a subcellular
259 compartment was calculated as the percentage of differentially distributed transcripts in a given
260 GO-category compared to the number of transcripts in the transcriptome in the same GO-
261 category. The hierarchical organization of the different enriched GO-terms were explored using
262 the Mouse Genome Informatics web page
263 (http://www.informatics.jax.org/vocab/gene_ontology). Heatmaps of GO terms showing the hit
264 percentage of significantly enriched GOs was constructed using the ComplexHeatmap package
265 in R (Gu et al., 2016), with a suitable number of K-means row-splitting. Row_km_repeats was
266 set to 100, which runs clustering multiple times and outputs the consensus cluster.

267

268 **Annotation of transcripts related to intracellular transport and localization**

269 Transcripts related to cytoskeletal components (Actin, Tubulin and related genes) and
270 cytoskeletal motor proteins (Myosins, Dyneins and Kinesins), and poly(A) polymerases, were
271 extracted from the eggNOG annotation. Homologs of genes related to cellular transport (COP
272 and Clathrin) were identified by reciprocal blast by using annotated genes in NCBI RefSeq
273 from *Chlamydomonas reinhardtii* as queries (see Table S4 for queries) against the *A.*
274 *acetabulum* transcriptome (blastp value cutoff < 0.0001). The resulting hits of the *A.*
275 *acetabulum* transcriptome were searched against Swissprot using blastp (evalue < 0.0001).
276 Transcripts which did not produce hits against Swissprot of the same category as in the first
277 blast search were discarded. Transcripts with a mean TMM-normalized CPM > 1 across all
278 samples were plotted, with standard error, using the R package ggplot2.

279

280 **Comparative transcriptomics between *A. acetabulum* and *Caulerpa taxifolia***

281 The *Caulerpa taxifolia* transcriptome (Ranjan et al., 2015) was translated into amino acid
282 sequences using Transdecoder v/3.0.0. Orthologous protein sequences between *A. acetabulum*
283 and *C. taxifolia* were identified using Orthofinder v/2.3.3 (Emms et al., 2015). RSEM generated
284 gene expression data from six different subcellular compartments of *C. taxifolia* (frond apex,
285 pinnules, rachis, frond base, stolon and holdfast) was downloaded from the supplementary
286 datafiles of Ranjan et al. (2015). The counts were rounded to the nearest integer and converted
287 to TMM-normalized counts (as described above). The TMM counts from the single-copy
288 orthologs from the different subcellular compartments of *A. acetabulum* and *C. taxifolia* were
289 merged and the differences in sample variation was visualized using the precomp function in R
290 and the ggplot2 R package.

291

292 **Results**

293 **Subcellular RNA isolation, sequencing and read processing**

294 The highest amount of total RNA was extracted from the cap samples (average of 252 ng),
295 followed by the upper stalk samples (average of 76 ng), the lower stalk (average of 46 ng), with
296 the lowest amount extracted from the rhizoid samples (average of 45 ng) (Table 1 and Figure
297 1B. The highest yield of total RNA was obtained using the “Total RNA purification kit” with
298 an elution volume of 40 ul (used for batch 26, 27, 45 and 46), which gave approximately four
299 times as much total RNA compared to the “Single Cell RNA purification kit” with an elution

300 volume of 10 ul (used for batch 17, 19 and 25) (Table S5). But still, the relative amounts of
301 RNA isolated from the different samples were the same regardless of the isolation kit.

302

303 The sequence reads from batch 17 had overall very low-quality scores as well as a high number
304 of duplicates (mostly from sequencing the adapters). Therefore, very few sequences were
305 retained after filtering and almost no genes were detected in these samples. The samples from
306 batch 17 were therefore discarded from further analyses. Between 14 and 43 million raw read
307 pairs were produced from each of the remaining 24 samples. Quality trimming and removal of
308 unpaired reads after trimming reduced the numbers by 13-25% for the majority of samples,
309 except for the Rhizoid of batch 26 and 27, where trimming reduced the number of reads by 40
310 and 49% (Table 1). Still, more than 15 million read pairs were left for these samples.

311

312 **Transcriptome assembly and annotation**

313 Assembling reads *de novo* produced an assembly consisting of 246,083 ‘genes’, or transcripts,
314 with a total of 429,781 different isoforms (Table S6), where the longest transcript was 17,196
315 bp and the shortest 201 bp. 245,334 transcripts were considered nuclear encoded, 389
316 transcripts gave hits against the chloroplast database and were considered to be chloroplast
317 encoded, 99 transcripts gave hits against the mitochondrial database and were considered
318 mitochondrial encoded. 261 gave hits against both the chloroplast and mitochondrial databases
319 and were considered as possible prokaryotic/unclassified transcripts as they also gave BLAST
320 hits against prokaryotic sequences against NCBI nr. 114,146 transcripts were predicted as
321 protein coding. Of these, 113,900 belonged to the nuclear genes, 178 to the chloroplast, and 68
322 to the mitochondria. 38,131 transcripts gave ortholog hits when analyzed by EggNOG, of where
323 18 779 transcripts were assigned GO-terms.

324

325 Assessing the presence of conserved eukaryotic genes in the transcriptome with a BUSCO
326 analysis estimated a ~96% completeness based on a pan-eukaryotic dataset and a ~70%
327 completeness based on a Chlorophyta dataset (Table 2). The pan-eukaryote dataset is much
328 smaller than the Chlorophyta dataset (303 genes vs. 2168 genes), which probably explains the
329 differences in the fraction of genes found. Nevertheless, these results indicate that our *de novo*
330 assembled transcriptome has captured the majority of the expressed genes in *Acetabularia*.

331

332

333 **RNA distribution**

334 For all 24 samples, more than 70% of the trimmed read pairs mapped to the transcriptome
335 (Table 1). There was no correlation between the number of mapped reads and the total UMI
336 count (Table 1), illustrating the extent of PCR duplication in the sequence libraries and the
337 importance of using UMIs. The majority of expressed transcripts were lowly expressed and 40-
338 50% of the expressed transcripts had a count of two or less.

339

340 The total UMI counts follow the same distribution as the amount of isolated total RNA, with
341 highest numbers in the cap samples and decreasing towards the rhizoid (Figure 1B and C). As
342 the dissected cap pieces were larger than the other pieces, it is also expected that the cap samples
343 contain the most RNA. However, as the same amount of RNA is sequenced from each library,
344 the size of the pieces, or the amount of isolated total RNA, cannot explain the higher count
345 values in the cap. This rather indicates a greater diversity, or heterogeneity, of transcripts in the
346 cap libraries compared to the other libraries.

347

348 While the nuclear encoded mRNAs had the same distribution as the total RNA, i.e. decreasing
349 towards the rhizoid (Figure S1A), ribosomal RNAs were roughly evenly distributed between
350 the different samples, although with a few extreme outliers (Figure S1B). Transcripts
351 presumably originating from the chloroplast were also distributed in an apical-basal gradient
352 (Figure S1C). Mitochondrial transcripts had the highest counts in the cap and the rhizoid (Figure
353 S1D), however these genes were much more variable between the samples and the counts were
354 also overall much lower and therefore more subjected to stochastic variation.

355

356 The principal component analysis (PCA) of the count variation between samples shows that the
357 samples largely cluster according to the cell apical-basal axis along PC1 (Figure 1D). This
358 shows that the cap- and the rhizoid are the least similar in transcript composition, while the two
359 stalk samples largely overlap and are fairly similar in terms of transcript expression. However,
360 there also seem to be a slight tendency that the samples cluster along PC2 according to which
361 batch they originate from (e.g. batch 19) or which RNA isolation method was used (e.g. batch
362 19 and 25 vs. batch 26, 27, 25 and 46). This indicates that also which batch of cells the samples
363 originated from (i.e. sampled at the same time), or which RNA isolation kit was used also
364 affects the sample variation.

365

366 **Table 1. Total RNA isolation and mRNA sequencing of subcellular fragments of *Acetabularia***
 367 ***acetabulum*.** The naming of samples is described in the text. Read numbers are given as pairs of reads
 368 (single reads were discarded), both before and after trimming. Mapping rate describes the percentage of
 369 paired reads mapping concordantly (i.e. mapping in the expected orientation relative to each other) to
 370 the *de novo* assembled transcriptome, total UMI count is the sum of transcript expression levels for each
 371 sample after removing PCR duplicates. Expressed transcripts shows the number of transcripts with at
 372 least one UMI count. % of expressed transcripts with count ≤ 2 is the percentage of “low count”
 373 transcripts.

Subcellular compartment	Batch	Total RNA (ng)	Raw reads (PE)	Trimmed reads (PE)	Mapped read pairs	Mapping rate (%)	Total UMI count	Expressed transcripts	% of transcripts with count ≤ 2
Cap	17	61	50 770 695	5 820 120	3 585 755	75	584	290	79
Upper stalk	17	29	82 587 170	11 714 864	7 206 886	73	660	257	68
Lower stalk	17	14	2 092	260	166	74	0	0	-
Rhizoid	17	36	38 755 094	18 101 837	11 382 777	75	475	167	51
Cap	19	95	25 526 511	19 934 510	12 521 349	76	8 010 785	62 257	44
Upper stalk	19	22	14 007 423	10 572 421	6 395 304	73	2 285 994	45 187	42
Lower stalk	19	11	18 869 617	14 309 848	8 742 817	74	656 729	30 620	43
Rhizoid	19	11	24 207 912	18 101 837	11 021 291	74	1 156 418	38 275	45
Cap	25	40	22 444 960	19 460 102	11 548 241	72	3 325 240	58 967	45
Upper stalk	25	30	31 098 736	26 710 669	15 574 348	73	4 547 527	57 122	43
Lower stalk	25	23	37 346 096	32 191 425	19 013 248	73	4 334 098	62 677	44
Rhizoid	25	18	37 858 071	32 519 937	19 919 778	73	3 466 028	58 615	48
Cap	26	132	32 643 222	28 358 416	16 777 807	72	4 656 581	63 592	44
Upper stalk	26	16	22 694 589	19 609 743	11 646 681	72	3 291 813	50 613	42
Lower stalk	26	51	37 555 049	32 280 766	19 117 797	73	1 307 014	39 224	43
Rhizoid	26	16	27 307 714	16 273 913	9 951 940	72	293 461	23183	39
Cap	27	187	27 859 229	21 702 199	13 055 825	72	6 704 550	77 998	45
Upper stalk	27	155	30 596 065	23 362 341	14 172 132	73	4 437 570	59 649	42
Lower stalk	27	63	25 217 910	19 013 147	11 575 387	73	2 137 899	45 753	43
Rhizoid	27	63	29 781 682	15 189 655	9 203 797	73	480 492	33 149	46
Cap	45	713	30 795 845	26 732 918	16 179 143	73	7 615 615	71 764	45
Upper stalk	45	72	28 618 780	24 538 566	14 672 568	74	2 949 290	55 172	47
Lower stalk	45	15	29 851 320	25 462 402	15 279 659	73	1 186 788	36 048	43
Rhizoid	45	49	43 496 924	36 991 784	22 472 939	73	2 078 673	44 095	44
Cap	46	534	43 691 338	37 748 810	22 697 840	72	10 250 494	79 349	44
Upper stalk	46	211	26 586 549	22 842 662	13 930 603	73	4 370 405	61 734	45
Lower stalk	46	144	29 167 985	25 131 292	15 639 747	73	6 189 014	64 045	46
Rhizoid	46	122	28 000 697	24 124 084	14 737 583	72	5 492 434	75 135	48

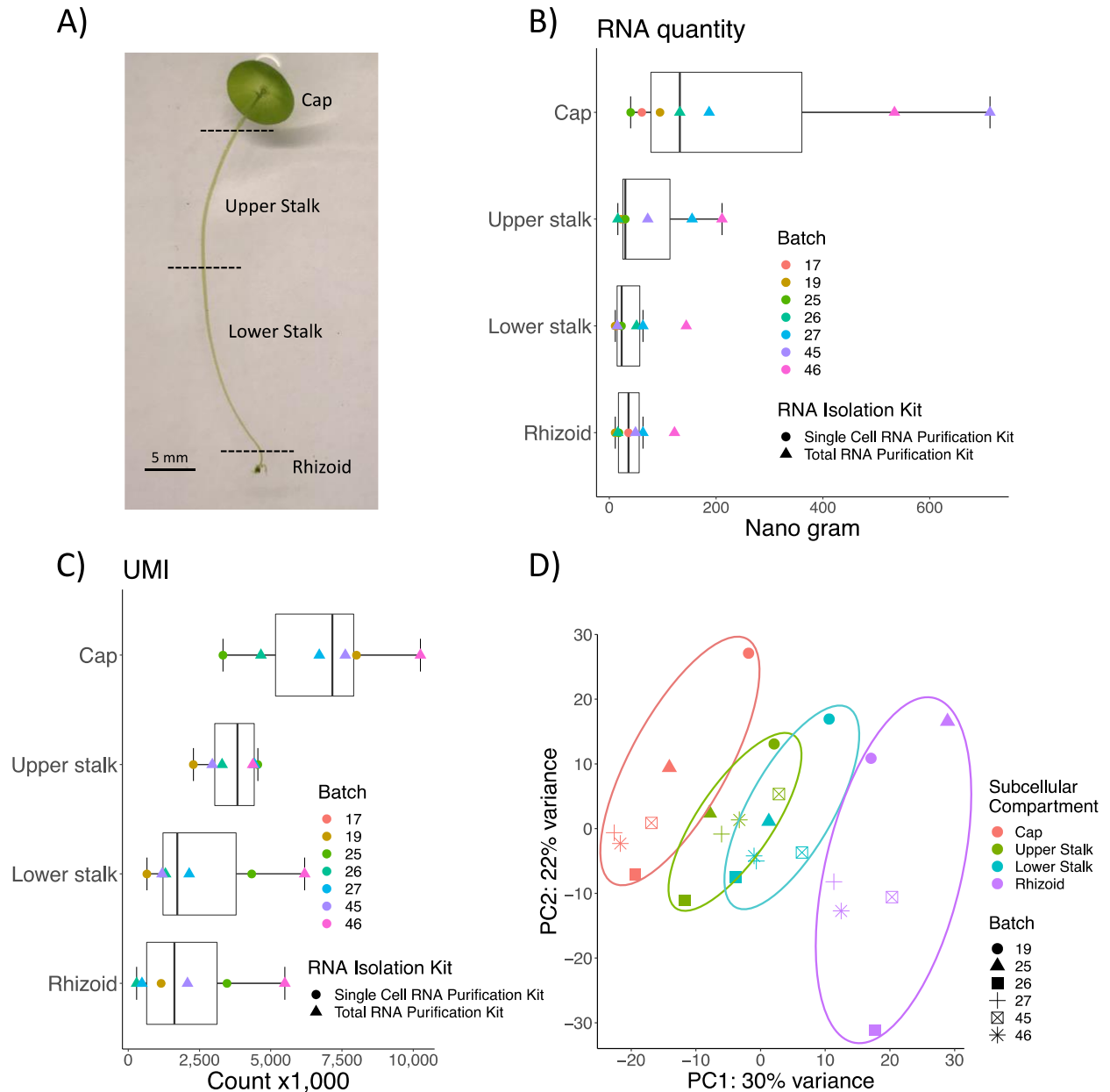
374
 375
 376
 377
 378
 379
 380
 381
 382
 383

384
385
386
387
388
389

Table 2. BUSCO analysis of the *de novo* assembled transcriptome of *A. acetabulum*. BUSCOs refer to the genes present in the different databases of the BUSCO software. Two datasets were used in our analysis, one containing 2168 genes conserved across Chlorophyta, and one containing 303 genes conserved across eukaryotes.

	Eukaryote BUSCO hits	Chlorophyta BUSCO hits
Complete BUSCOs	245 (80.9%)	1349 (62.2%)
Single-copy	159 (52.5%)	1047 (48.3%)
Duplicated	86 (28.4%)	302 (13.9%)
Fragmented BUSCOs	45 (14.9%)	177 (8.2%)
Missing BUSCOs	13 (4.2%)	642 (29.6%)
Total BUSCOs searched	303	2168

390
391
392
393
394
395
396
397



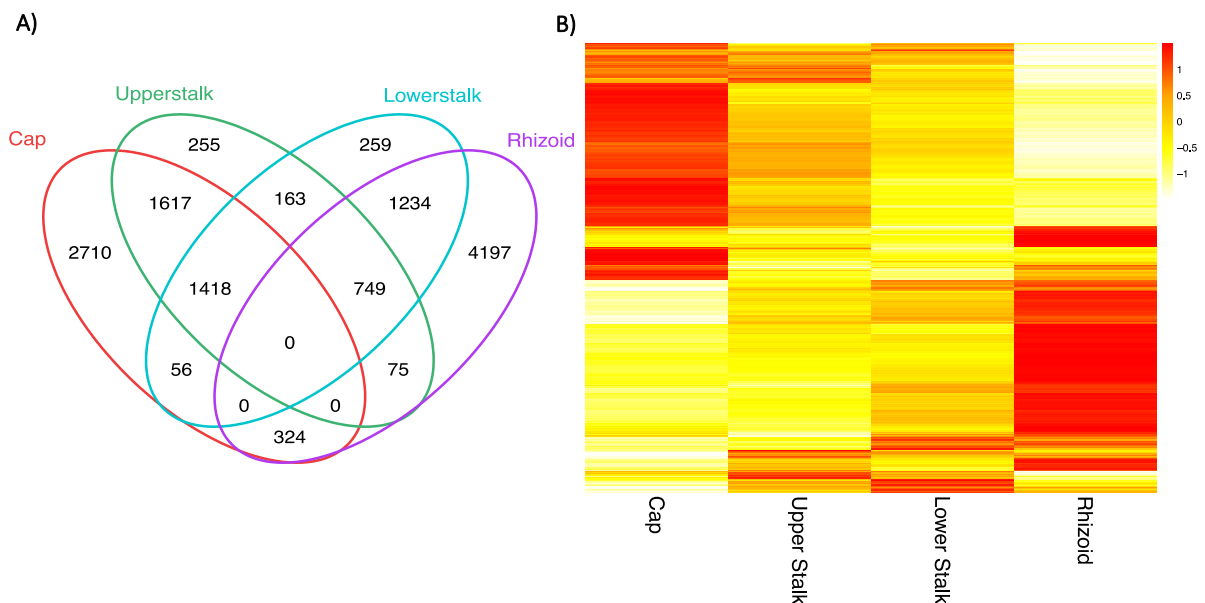
398
399
400
401
402
403
404
405
406
407
408
409
410
411
412
413
414

Figure 1. RNA isolation and sequencing of subcellular compartments of adult *A. acetabulum*. A) Image of an adult cell of *A. acetabulum*. The dashed lines indicate approximate incision sites for separating the different subcellular sections; cap, upper stalk, lower stalk and rhizoid. B) Boxplot showing the total RNA quantity isolated from the different subcellular compartments. The dots represent the individual samples colored according to which batch the sample originate from, and shaped according to which RNA isolation kit that was used. C) Boxplot showing the summarized gene expression levels (total UMI counts) of the different samples. The dots are the same as above. D) Principal Component Analysis (PCA) of the sample variation based on variance stabilized counts (see Methods). The four subcellular compartments are shown in color, and the different batches which the samples originate from (described in the Methods) are indicated as shapes.

415 Differential transcript distribution

416 The majority of the assembled transcripts were expressed at low levels (which is expected as
417 transcriptomes assembled *de novo* from NGS data always contains a high number of assembly
418 artefacts and wrongly assembled isoforms). 87% of the transcripts had a mean expression of >1
419 TMM across the samples, and filtering nuclear encoded transcripts with a raw count of one or
420 more in at least four samples retained 82,164 transcripts. Out of these, 13,057 transcripts were
421 identified as significantly differentially distributed between at least two subcellular
422 compartments. Of the differentially distributed transcripts, 4,197 transcripts were uniquely
423 located in the rhizoid, 2,710 transcripts were unique to the cap, and 255 and 259 transcripts
424 were uniquely located in the upper- and lower stalk respectively (Figure 2A). 1,617 transcripts
425 were enriched in both the cap and the upper stalk, 163 transcripts in both the upper- and lower
426 stalk, and 1,234 transcripts were enriched in both the lower stalk and the rhizoid. Visualizing
427 the expression of these differentially distributed transcripts (Figure 2B) confirms the clustering
428 analysis in that there are two large and distinct pools of enriched transcripts in the cap and the
429 rhizoid, and that these subcellular compartments are the least similar in terms of gene content.
430 The upper- and lower stalk samples have similar expression profiles and share a large number
431 of differentially distributed transcripts. These two compartments also have an overall lower
432 gene expression compared to the cap and rhizoid.

433

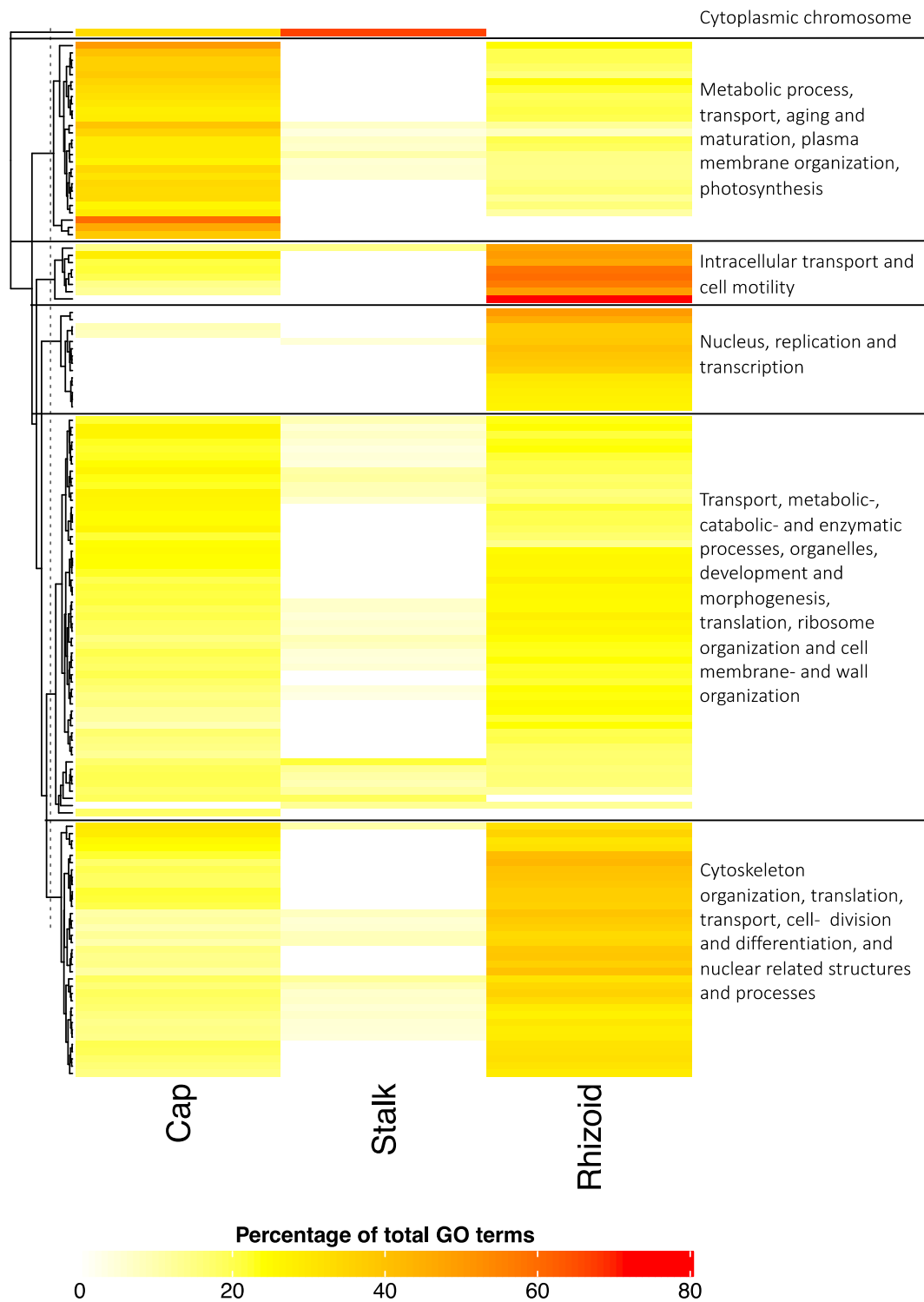


434
435 **Figure 2. Differentially distributed transcripts between the subcellular compartments.** A) Venn
436 diagram showing the shared and unique number of transcripts that are differentially distributed between
437 the subcellular compartments. B) Heatmap of the differentially distributed transcripts. Colors represent
438 scaled TMM (Trimmed Mean of M-values) expression values. The mean TMM values across the
439 different samples from each subcellular structure is shown.

440 **GO enrichment**

441 In order to investigate which genetic processes were taking place in the different subcellular
442 compartments, we analyzed the different subcellular pools of nuclear encoded transcripts for
443 the presence of enriched functional categories. As the two stalk samples displayed very similar
444 expression patterns, they were analyzed together (referred to as “stalk”) to get a clearer picture
445 of the differences between the stalk, cap and the rhizoid. The GO-enrichment analysis resulted
446 in 126 enriched GO-terms in the cap, 134 in the rhizoid, and 57 in the stalk (there were eight
447 enriched GO-terms in the upper stalk and 14 in the lower stalk when analyzed separately) (Table
448 S7).

449
450 Nuclear encoded mRNA transcripts accumulating in the cap were enriched for GO-terms
451 related to photosynthesis such as photosynthetic processes, chloroplast components and
452 thylakoid (Figure 3). General metabolic processes, organization of the plasma membrane and
453 extracellular matrix, development and transport were also enriched in the cap, and to a lesser
454 extent enriched in the rhizoid. No particular processes seemed to be unique to the stalk.
455 However, the GO-term “cytoplasmic chromosome”, which was also enriched in the cap, was
456 significantly enriched in the stalk, and GO-terms related to metabolic processes, catalytic
457 activity, cellular organelles and transport was to small degree enriched in the stalk. Nuclear
458 encoded mRNA transcripts accumulating in the rhizoid were enriched for GO-terms related to
459 the nucleus, replication, transcription, and cell motility. In addition, cytoskeleton organization
460 and cell- division and differentiation were enriched in the rhizoid and also to a lesser extent in
461 the cap. Other processes which seemed to be more widely distributed and which were enriched
462 in both the cap and the rhizoid were related to, transport, translation, ribosome organization,
463 cell wall- and cell membrane organization, development and morphogenesis, and general
464 metabolic and enzymatic processes.



465

466

467

468

469

470

471

472

473

474

Figure 3. GO-enrichment analysis of transcripts differentially distributed between subcellular compartments. Heatmap of the enriched GO-terms among the differentially distributed transcripts in each subcellular compartment (note that the stalk samples are analyzed together). The colors indicate the percentage of differentially distributed transcripts annotated with a given GO-category compared to the total number of transcripts in the same GO-category. All GO-categories (Biological Process, Cellular Compartment and Molecular Function) are shown together. A GO-term not significantly enriched in a subcellular compartment is set to zero percent (hence shown in white color). The most prevalent GO-terms have been simplified and highlighted on the right side of the heatmap. See table S7 for a full description of the GO-enrichment results.

475

476 **Distribution of genes involved in mRNA compartmentalization**

477 Analyses of the mRNA distribution indicated the presence of functionally related subcellular
478 pools of transcripts. Therefore, we investigated in detail the distribution patterns of transcripts
479 potentially involved in generating this type of distribution.

480

481 Transcripts related to the cytoskeleton, such as actin and tubulin, are highly abundant along the
482 entire cell, and apparently not specifically associated with any particular subcellular region
483 (Figure 4A and B). Transcripts encoding motor proteins moving along the cytoskeleton such as
484 myosin, dynein and kinesin, are also present throughout the cell, although not as evenly
485 distributed as the cytoskeletal components (Figure 4C-E). Myosin transcripts were more
486 abundant in the apical end and decreasing towards the rhizoid. This includes class XIII myosin
487 which have been shown to be involved in organelle transport and tip growth in *A. cliftonii* and
488 enriched in the apical regions of the cell (Vugrek et al., 2003). The same trend was observed
489 also for kinesins, except for two transcripts which were most abundant in the rhizoid.
490 Interestingly, these two transcripts have the closest blast hits against kinesin 13 and 14, which
491 are known to move in both directions on the microtubule, and can thereby travel in the opposite
492 direction on the microtubules than the other kinesins.

493

494 In contrast, the dyneins were overall lesser expressed than myosins and kinesins. The most
495 highly abundant dynein was present through the cell in roughly equal amounts, while the rest
496 of the transcripts were most abundant in the rhizoid. Myosins and kinesin generally move
497 towards the plus-ends of the polarized actin microfilaments and microtubules respectively, and
498 thus from the nucleus towards the cell membrane. While dyneins move toward the minus end
499 of microtubules towards the cell interior (Alberts et al., 2002). Hence, motor proteins moving
500 towards the cell membrane are of a slightly higher abundance in the apical part of the cell
501 (except from two kinesin transcripts which are of a higher abundance in the basal part of the
502 cell), while motor proteins moving towards the cellular interior are seemingly of a higher
503 abundance in the basal part of the cell (lower stalk and rhizoid).

504

505 Vesicular transport is a fundamental mechanism for intracellular transport of cargo
506 in eukaryote cells, and has been associated with intracellular transport of RNA (Basyuk et al.,
507 2003; Roberts et al., 2013; Skog et al., 2008). Vesicle formation relies on coat proteins, and
508 COPI- COPII- and Clathrin coated vesicles are the main type of vesicles in eukaryote cells.

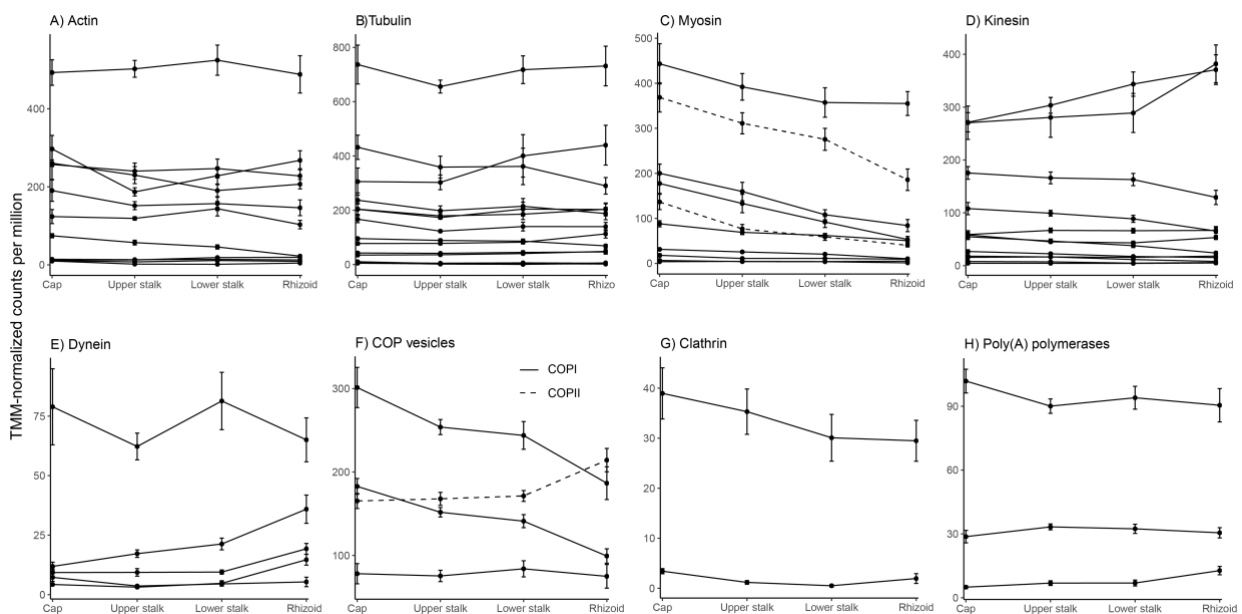
509 COPI-coated vesicles move from ER to golgi, COPII-coated vesicles move between parts of
 510 golgi and retrograde transport from golgi to ER, and Clathrin-coated vesicles move from golgi
 511 to the plasma membrane (Gomez-Navarro et al., 2016). In our results, two of three COPI
 512 transcripts were most abundant in the cap and decrease towards the rhizoid, while one COPII
 513 transcript was most abundant in the rhizoid (Figure 4F). Two Clathrin homologs were
 514 distributed throughout the cell, one of these transcripts was of noticeable higher abundance than
 515 the other (Figure 4G). This high abundant transcript was also of a slightly higher concentration
 516 in the cap and decreasing towards the rhizoid.

517

518 Three copies of poly(A) polymerases were expressed in *A. acetabulum*. All three were evenly
 519 distributed throughout the cell, however one was higher expressed than the others (Figure 4H).

520

521



522

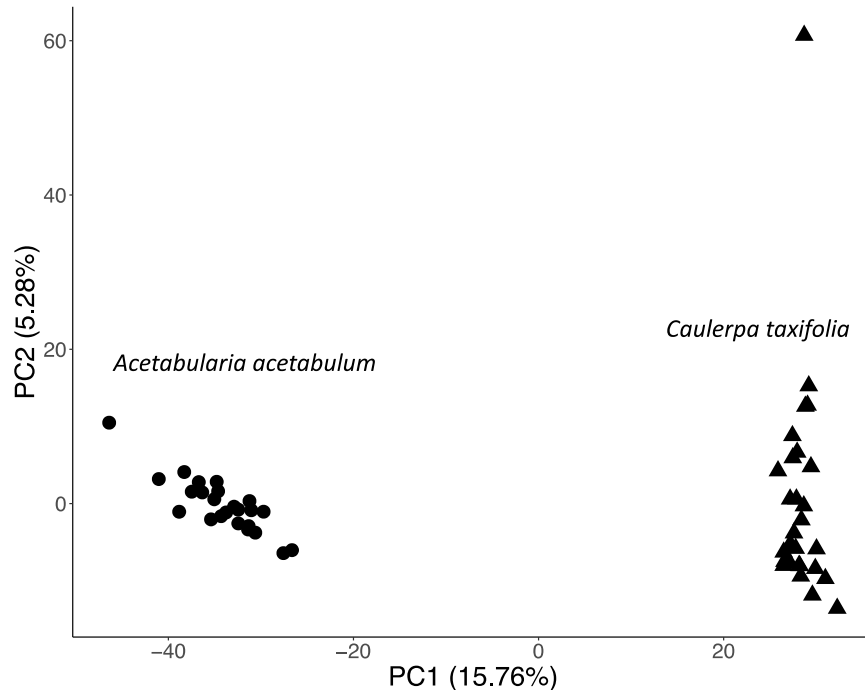
523 **Figure 4. Distribution of transcripts related to transport and RNA localization.** The distribution of
 524 homologs of Actin (A), Tubulin (B), Myosin (C) – the dashed lines indicates homologs of Class XIII
 525 myosin identified in *A. cliftonii*, Kinesin (D), Dynein (E), genes creating COP vesicles (F), Clathrin (G)
 526 and poly(A) polymerases (H). Expression values (TMM-normalized counts per million) are shown on
 527 the y-axis, with error bars representing standard error. Only transcripts with a mean normalized
 528 expression >1 across all samples are shown.

529

530 **Comparative transcriptomics between *A. acetabulum* and *Caulerpa taxifolia***

531 Orthology searches between the transcriptomes of *A. acetabulum* and *Caulerpa taxifolia*
 532 resulted in 4,483 orthogroups represented by at least one transcript from each species. Of these
 533 orthogroups, 2,120 were single-copy orthologues with a single representative from each

534 species. Comparison of the different samples from the two species based on expression
535 dynamics of these single-copy orthologues showed that the genes clustered strongly according
536 to species, rather than to subcellular compartment between species (Figure 5).
537



538
539 **Figure 5. Comparison of the expression profile of gene orthologues between *A. acetabulum* and *C.***
540 ***taxifolia*.** Principal Component Analysis (PCA) of the sample variation based on TMM-normalized
541 counts per million (see Methods) of single-copy orthologues between *A. acetabulum* (circles) and *C.*
542 *taxifolia* (triangles).
543

544

545 Discussion

546 Apical-basal mRNA gradient in *A. acetabulum*

547 *Acetabularia acetabulum* has been used as a model system for cell morphogenesis for decades,
548 and it has been suspected that differential distribution of RNA long the cell axis is an underlying
549 mechanism for its sophisticated morphology (Dumais et al., 2000; Hämmerling, 1934b;
550 Serikawa et al., 2001; Vogel et al., 2002). To investigate the distribution of mRNA in adult *A.*
551 *acetabulum* cells we have performed subcellular mRNA sequencing and functional enrichment
552 analysis. We have tagged each mRNA molecule with unique molecular indexes (UMIs) which
553 allows for true quantification of mRNA by eliminating the effect of amplification bias
554 introduced during library preparation. Despite isolating RNA from subsections of a single-cell,
555 we were able to capture the majority of expressed transcripts, and although there is some

556 variation between samples the procedure was repeatable and robust even to the type of RNA
557 isolation protocols.

558
559 Our results demonstrate the presence of RNA throughout the entire cell length, and identified
560 the highest amount of mRNA at the apical end of the cell (the cap) decreasing towards the basal
561 end (the rhizoid), confirming earlier discoveries of an apical-basal gradient of RNA in *A.*
562 *acetabulum* (Baltus et al., 1968; Hämmerling, 1936; Werz, 1955). However, while it has been
563 believed that this gradient is due to different concentrations of RNA encoded by the
564 chloroplasts, and not nuclear encoded RNAs (Naumova et al., 1976), we rather find that the
565 apical-basal gradient is mainly caused by nuclear encoded mRNAs.

566
567 **Localized pools of transcripts support subcellular mRNA compartmentalization**

568 A long-standing question has been whether the observed gradient of mRNA in *A. acetabulum*
569 is homogeneous in transcript composition, or whether there are distinct pools of transcripts
570 along the cell. Hämmerling's grafting experiments suggested the existence of local
571 determinants of morphogenesis, and Dumais et al. (2000) speculated that mRNAs would either
572 be distributed throughout the cell, or localized to the apical or basal ends. Our results show that
573 while some gene transcripts are distributed evenly across the entire cell, a large part are actually
574 abundantly located to different subcellular compartments. We also found that these pools of
575 transcripts are composed of functionally related transcripts. Transcripts related to
576 photosynthesis are co-localized and accumulated in the apical end of the cell, while transcripts
577 related to nuclear processes co-localized in the basal end. This pattern shows that the RNA
578 gradient is not a homogeneous mix of gene transcripts, which confirms that mechanisms to
579 ensure specific and functional RNA localization must be in place in *A. acetabulum*.

580
581 There were overall fewer transcripts localized in the stalk. This was not surprising as the stalk
582 is mainly filled with a central vacuole, with only a thin layer of cytoplasm covering it (Dumais
583 et al., 2000), leaving very little room for other subcellular structures or pools of transcripts. We
584 therefore assume that there are very few processes happening exclusively in the stalk and that
585 the stalk might even function as a physical border between the cap and the rhizoid, making sure
586 that molecules and other substances are not mixed between the two compartments, but instead
587 carefully transported between them.

588
589

590 **Active mRNA transport is likely the main mechanism for establishment of cell polarity**

591 RNA can be distributed around a cell either by passive diffusion from the nucleus, or by active
592 transport along the cytoskeleton (St Johnston, 2005). Studies tracking the movement of
593 radioactive labelled RNA labelled have shown that mRNA travel faster in *A. acetabulum* than
594 what is possible by diffusion alone (Kloppstech et al., 1975b), and simply the size of the cell,
595 with the nucleus and the cap separated by several centimeters, puts obvious demands on active
596 intracellular transport. A highly sophisticated and extensively developed cytoskeleton has been
597 overserved in *A. acetabulum*, with large tracks of actin filaments running the entire length of
598 the cell (Menzel, 1994). Experiments by Mine et al. (2001) showed that inhibiting actin
599 polymerization with cyclohalasin D disrupts the established mRNA gradients, indicating that
600 there is an association between mRNA and the cytoskeleton. As expected, we find that
601 transcripts encoding the main cytoskeletal components such as actin and tubulin are uniformly
602 distributed throughout the cell. Furthermore, we see that both Clathrin and COP genes, as well
603 as homologs of motor proteins traveling in both directions on the cytoskeleton, are distributed
604 throughout the cell, suggesting that these types of vesicular transport systems are active in the
605 entire cell.

606

607 **mRNA stabilization and post-transcriptional control**

608 The fact that some transcripts are evenly distributed while others are localized, implies that the
609 cell is either able to distinguish between which mRNAs should be transported where, but can
610 also mean that there are mechanisms for selective stabilization and degradation of mRNAs at
611 different locations in the cell. While actin microfilaments are present throughout the cell for the
612 entire life cycle of *A. acetabulum*, microtubules do not appear until the final stages of
613 development where they serve as transport tracks in the cap (Menzel, 1986; Menzel, 1994).
614 This is interesting as tubulin genes are expressed much earlier and distributed throughout the
615 cell, so tubulin mRNAs must be stabilized and stored in the cytoplasm and prevented from
616 being translated. That mRNA is long-lived in *A. acetabulum* cells is supported by experiments
617 showing that development and morphogenesis can continue for days, and even weeks, after
618 amputation of the nucleus (Stich et al., 1958; Yasinovski et al., 1979), and that radioactive
619 RNAs exist in *A. acetabulum* cells long after treatment with radioactive labelled UTP
620 (Kloppstech et al., 1982; Schweiger, 1977). It is also interesting that we find polyadenylation
621 genes distributed throughout the cell, as editing, shortening and elongation of the poly-A-tail is
622 an important mechanism for translational control (Aphasizhev, 2005; Wickens, 1992).

623

624 **The cap is the main morphogenetic and metabolic structure**

625 The GO-enrichment analysis also shows a higher level of catalytic- and metabolic activity in
626 the cap compared the rhizoid, indicating the cap is the metabolically more diverse and active
627 region of the cell. We also see the greatest diversity of expressed transcripts in the cap, and the
628 highest overall RNA content. These finding agree with earlier observations that the cap is the
629 section of the cell with the highest morphogenetic capacity, or developmental potential, as it
630 can regenerate both whorls of hair and the entire cap structure after being dissected from the
631 rhizoid (Menzel, 1994; Serikawa et al., 2001), while the nucleus is mostly the place for
632 production of mRNAs and replication.

633

634 **Ortholog comparison indicates little genetic homology between subcellular sections of *A.***
635 ***acetabulum* and *Caulerpa taxifolia***

636 *Caulerpa taxifolia* is another Chlorophyte algae with many similarities to *A. acetabulum*, most
637 notably they are both gigantic single-celled species with highly complex cellular morphologies
638 with clearly distinguished apical and basal ends. However, unlike *A. acetabulum*, *C. taxifolia*
639 is a syncytium with hundreds, or even thousands, of nuclei scattered throughout the cell. Ranjan
640 et al. (2015) characterized the gene expression patterns of the different subcellular sections of
641 *C. taxifolia* and found that they contained unique expression profiles, similar to what we see in
642 *A. acetabulum*. However, comparing the expression profile of single-copy orthologs between
643 the two species shows that the subcellular sections are more similar within each species rather
644 than between species, indicating that there are different genes active in the apical and basal
645 sections in these two species, and hence little homology at the genetic level. Nevertheless,
646 comparing the functional annotations of these genes indeed shows some similarities. Both
647 species are enriched for nuclear components and DNA-related processes, such as DNA
648 replication and transcription in the basal parts of the algae, as well as displaying a higher
649 catalytic activity in the apical parts (Ranjan et al., 2015). Therefore, although morphologically
650 similar cell sections of these two species contain largely non-orthologous mRNAs, they do
651 seem to share overall similar genetic functions. This might be an indication of evolutionary
652 convergence on a functional level in the two species.

653

654

655

656

657 **References**

- 658 Alberts, B., Johnson, A., Lewis, J., Martin, R., Roberts, K., & Walter, P. (2002). *Molecular*
659 *Biology of the Cell* (4 ed.). New York: Garland Science.
- 660 Aphasizhev, R. (2005). RNA uridylyltransferases. *Cell Mol Life Sci*, 62(19-20), 2194-2203.
661 doi:10.1007/s00018-005-5198-9
- 662 Arimoto, A., Nishitsuji, K., Higa, Y., Arakaki, N., Hisata, K., Shinzato, C., . . . Shoguchi, E.
663 (2019). A siphonous macroalgal genome suggests convergent functions of homeobox
664 genes in algae and land plants. *DNA Res*, 26(2), 183-192. doi:10.1093/dnares/dsz002
- 665 Bacher, R., Chu, L. F., Leng, N., Gasch, A. P., Thomson, J. A., Stewart, R. M., . . . Kendzioriski, C.
666 (2017). SCnorm: robust normalization of single-cell RNA-seq data. *Nature Methods*,
667 14(6), 584+. doi:DOI 10.1038/nmeth.4263
- 668 Backman, T. W. H., & Girke, T. (2016). systemPipeR: NGS workflow and report generation
669 environment. *BMC Bioinformatics*, 17, 388. doi:10.1186/s12859-016-1241-0
- 670 Baltus, E., Edstrom, J. E., Janowski, M., Hanocquq, J., Tencer, R., & Brachet, J. (1968). Base
671 Composition and Metabolism of Various Rna Fractions in Acetabularia Mediterranea.
672 *Proc Natl Acad Sci U S A*, 59(2), 406+. doi:DOI 10.1073/pnas.59.2.406
- 673 Basyuk, E., Galli, T., Mougél, M., Blanchard, J. M., Sitbon, M., & Bertrand, E. (2003).
674 Retroviral genomic RNAs are transported to the plasma membrane by endosomal
675 vesicles. *Developmental Cell*, 5(1), 161-174. doi:Doi 10.1016/S1534-5807(03)00188-6
- 676 Berger, S. (1990). Dasycladaceae - a family of giant unicellular algae ideal for research.
677 *Experimental Embryology in Aquatic Plants and Animals*, 195, 3-19. doi:10.1007/978-
678 1-4615-3830-1_1
- 679 Berger, S. (2006). *Photo-Atlas og living Dasycladales: Carnets de Geologie*.
- 680 Bolger, A. M., Lohse, M., & Usadel, B. (2014). Trimmomatic: a flexible trimmer for Illumina
681 sequence data. *Bioinformatics*, 30(15), 2114-2120.
682 doi:10.1093/bioinformatics/btu170
- 683 Bushnell, B. (2015). *BBMap short-read aligner, and other bioinformatics tools*.
- 684 Dumais, J., Serikawa, K., & Mandoli, D. F. (2000). Acetabularia: A Unicellular Model
685 for Understanding Subcellular Localization and Morphogenesis during Development.
686 *Journal of Plant Growth Regulation*, 19(3), 253-264. doi:10.1007/s003440000035
- 687 Emms, D. M., & Kelly, S. (2015). OrthoFinder: solving fundamental biases in whole genome
688 comparisons dramatically improves orthogroup inference accuracy. *Genome Biology*,
689 16. doi:ARTN 157
690 10.1186/s13059-015-0721-2
- 691 Garcia, E., & Dazy, A. C. (1986). Spatial-Distribution of Poly(a)+ Rna and Protein-Synthesis in
692 the Stalk of Acetabularia-Mediterranea. *Biology of the Cell*, 58(1), 23-29. Retrieved
693 from <Go to ISI>://WOS:A1986F879300003
- 694 Gomez-Navarro, N., & Miller, E. A. (2016). COP-coated vesicles. *Current Biology*, 26(2), R54-
695 R57. doi:10.1016/j.cub.2015.12.017
- 696 Grabherr, M. G., Haas, B. J., Yassour, M., Levin, J. Z., Thompson, D. A., Amit, I., . . . Regev, A.
697 (2011). Full-length transcriptome assembly from RNA-Seq data without a reference
698 genome. *Nature Biotechnology*, 29(7), 644-U130. doi:10.1038/nbt.1883
- 699 Gu, Z. G., Eils, R., & Schlesner, M. (2016). Complex heatmaps reveal patterns and
700 correlations in multidimensional genomic data. *Bioinformatics*, 32(18), 2847-2849.
701 doi:10.1093/bioinformatics/btw313

- 702 Huerta-Cepas, J., Forslund, K., Coelho, L. P., Szklarczyk, D., Jensen, L. J., von Mering, C., &
703 Bork, P. (2017). Fast Genome-Wide Functional Annotation through Orthology
704 Assignment by eggNOG-Mapper. *Molecular Biology and Evolution*, *34*(8), 2115-2122.
705 doi:10.1093/molbev/msx148
- 706 Huerta-Cepas, J., Szklarczyk, D., Heller, D., Hernandez-Plaza, A., Forslund, S. K., Cook, H., . . .
707 Bork, P. (2019). eggNOG 5.0: a hierarchical, functionally and phylogenetically
708 annotated orthology resource based on 5090 organisms and 2502 viruses. *Nucleic
709 Acids Research*, *47*(D1), D309-D314. doi:10.1093/nar/gky1085
- 710 Hämmerling, J. (1934a). On genome effects and formation ability in Acetabularia. *Wilhelm
711 Roux Archiv Fur Entwicklungsmechanik Der Organismen*, *132*(2/3), 424-462.
712 Retrieved from <Go to ISI>://WOS:000200165400004
- 713 Hämmerling, J. (1934b). On substances determining the development in Acetabularia
714 mediterranea, their spatial and temporal distribution and origin. *Wilhelm Roux Archiv
715 Fur Entwicklungsmechanik Der Organismen*, *131*(1), 1-81. Retrieved from <Go to
716 ISI>://WOS:000200164900001
- 717 Hämmerling, J. (1934c). Physiological development and genetic foundation of the form
718 creation in the shielding algae Acetabularia. *Naturwissenschaften*, *32*, 829-836.
719 Retrieved from <Go to ISI>://WOS:000200261600132
- 720 Hämmerling, J. (1936). Studien zum Polaritätsproblem. *Zoologische Jahrbücher*, *56*, 441-483.
- 721 Hämmerling, J. (1953). Nucleo-cytoplasmic Relationships in the Development of
722 Acetabularia. In G. H. Bourne & J. F. Danielli (Eds.), *International Review of Cytology*
723 (Vol. 2, pp. 475-498): Academic Press.
- 724 Hämmerling, J. (1963). *Nucleo-Cytoplasmic Interactions in Acetabularia and other Cells* (Vol.
725 14): Annu. Rev. Plant Physiol.
- 726 Haas, B. J., Papanicolaou, A., Yassour, M., Grabherr, M., Blood, P. D., Bowden, J., . . . Regev,
727 A. (2013). De novo transcript sequence reconstruction from RNA-seq using the Trinity
728 platform for reference generation and analysis. *Nat Protoc*, *8*(8), 1494-1512.
729 doi:10.1038/nprot.2013.084
- 730 Jukes, T. H. (1996). Neutral changes and modifications of the genetic code. *Theoretical
731 Population Biology*, *49*(2), 143-145. doi:DOI 10.1006/tpbi.1996.0008
- 732 Kaplan, D. R. (1992). The Relationship of Cells to Organisms in Plants - Problem and
733 Implications of an Organismal Perspective. *International Journal of Plant Sciences*,
734 *153*(3), S28-S37. doi:Doi 10.1086/297061
- 735 Kaplan, D. R., & Hagemann, W. (1991). The Relationship of Cell and Organism in Vascular
736 Plants - Are Cells the Building-Blocks of Plant Form. *Bioscience*, *41*(10), 693-703.
737 doi:Doi 10.2307/1311764
- 738 Klopstech, K. (1977). Messenger-Type Rna from Acetabularia. *Protoplasma*, *91*(2), 224-224.
739 Retrieved from <Go to ISI>://WOS:A1977DB40900018
- 740 Klopstech, K., & Schweiger, H. G. (1975a). 80 S ribosomes in Acetabularia major.
741 Distribution and transportation within the cell. *Protoplasma*, *83*(1-2), 27-40.
742 Retrieved from <https://www.ncbi.nlm.nih.gov/pubmed/1118628>
- 743 Klopstech, K., & Schweiger, H. G. (1975b). Polyadenylated Rna from Acetabularia.
744 *Differentiation*, *4*(3), 115-123. doi:DOI 10.1111/j.1432-0436.1975.tb01450.x
- 745 Klopstech, K., & Schweiger, H. G. (1982). Stability of poly(A)(+)RNA in nucleate and
746 anucleate cells of Acetabularia. *Plant Cell Rep*, *1*(4), 165-167.
747 doi:10.1007/BF00269189

- 748 Langmead, B., & Salzberg, S. L. (2012). Fast gapped-read alignment with Bowtie 2. *Nat*
749 *Methods*, 9(4), 357-359. doi:10.1038/nmeth.1923
- 750 Love, M. I., Huber, W., & Anders, S. (2014). Moderated estimation of fold change and
751 dispersion for RNA-seq data with DESeq2. *Genome Biology*, 15(12), 550.
752 doi:10.1186/s13059-014-0550-8
- 753 McCarthy, D. J., Chen, Y. S., & Smyth, G. K. (2012). Differential expression analysis of
754 multifactor RNA-Seq experiments with respect to biological variation. *Nucleic Acids*
755 *Research*, 40(10), 4288-4297. doi:10.1093/nar/gks042
- 756 Menzel, D. (1986). Visualization of Cytoskeletal Changes through the Life-Cycle in
757 *Acetabularia*. *Protoplasma*, 134(1), 30-42. doi:Doi 10.1007/Bf01276373
- 758 Menzel, D. (1994). Cell differentiation and the cytoskeleton in *Acetabularia*. *New Phytologist*,
759 128(3), 369-393. doi:10.1111/j.1469-8137.1994.tb02984.x
- 760 Mine, I., Okuda, K., & Menzel, D. (2001). Poly(A)(+) RNA during vegetative development of
761 *Acetabularia peniculus*. *Protoplasma*, 216(1-2), 56-65. doi:Doi 10.1007/Bf02680131
- 762 Naumova, L. P., Pressman, E. K., & Sandakchiev, L. S. (1976). Gradient of Rna Distribution in
763 Cytoplasm of *Acetabularia-Mediterranea*. *Plant Science Letters*, 6(4), 231-235. doi:Doi
764 10.1016/0304-4211(76)90052-3
- 765 Niklas, K. J., Cobb, E. D., & Crawford, D. R. (2013). The evo-devo of multinucleate cells,
766 tissues, and organisms, and an alternative route to multicellularity. *Evolution &*
767 *Development*, 15(6), 466-474. doi:10.1111/ede.12055
- 768 Ranjan, A., Townsley, B. T., Ichihashi, Y., Sinha, N. R., & Chitwood, D. H. (2015). An
769 intracellular transcriptomic atlas of the giant coenocyte *Caulerpa taxifolia*. *PLoS*
770 *Genet*, 11(1), e1004900. doi:10.1371/journal.pgen.1004900
- 771 Roberts, C. T., Jr., & Kurre, P. (2013). Vesicle trafficking and RNA transfer add complexity and
772 connectivity to cell-cell communication. *Cancer Res*, 73(11), 3200-3205.
773 doi:10.1158/0008-5472.CAN-13-0265
- 774 Robinson, M. D., McCarthy, D. J., & Smyth, G. K. (2010). edgeR: a Bioconductor package for
775 differential expression analysis of digital gene expression data. *Bioinformatics*, 26(1),
776 139-140. doi:10.1093/bioinformatics/btp616
- 777 Schneider, S. U., Leible, M. B., & Yang, X. P. (1989). Strong Homology between the Small
778 Subunit of Ribulose-1,5-Bisphosphate Carboxylase Oxygenase of 2 Species of
779 *Acetabularia* and the Occurrence of Unusual Codon Usage. *Molecular and General*
780 *Genetics*, 218(3), 445-452. doi:Doi 10.1007/Bf00332408
- 781 Schweiger, H.-G. (1977). Transcription of the Nuclear Genome of *Acetabularia*. In L. Bogorad
782 & J. H. Weil (Eds.), *Nucleic Acids and Protein Synthesis in Plants* (pp. 65-83). Boston,
783 MA: Springer US.
- 784 Serikawa, K. A., & Mandoli, D. F. (1999). Aaknox1, a kn1-like homeobox gene in *Acetabularia*
785 acetabulum, undergoes developmentally regulated subcellular localization. *Plant Mol*
786 *Biol*, 41(6), 785-793.
- 787 Serikawa, K. A., Porterfield, D. M., & Mandoli, D. F. (2001). Asymmetric subcellular mRNA
788 distribution correlates with carbonic anhydrase activity in *Acetabularia acetabulum*.
789 *Plant Physiology*, 125(2), 900-911. doi:DOI 10.1104/pp.125.2.900
- 790 Simao, F. A., Waterhouse, R. M., Ioannidis, P., Kriventseva, E. V., & Zdobnov, E. M. (2015).
791 BUSCO: assessing genome assembly and annotation completeness with single-copy
792 orthologs. *Bioinformatics*, 31(19), 3210-3212. doi:10.1093/bioinformatics/btv351
- 793 Skog, J., Wurdinger, T., van Rijn, S., Meijer, D. H., Gainche, L., Sena-Estevés, M., . . .
794 Breakefield, X. O. (2008). Glioblastoma microvesicles transport RNA and proteins that

795 promote tumour growth and provide diagnostic biomarkers. *Nature Cell Biology*,
796 10(12), 1470-U1209. doi:10.1038/ncb1800

797 St Johnston, D. (2005). Moving messages: The intracellular localization of mRNAs. *Nature*
798 *Reviews Molecular Cell Biology*, 6(5), 363-375. doi:10.1038/nrm1643

799 Stich, H., & Plaut, W. (1958). The effect of ribonuclease on protein synthesis in nucleated
800 and enucleated fragments of *Acetabularia*. *J Biophys Biochem Cytol*, 4(1), 119-121.
801 doi:10.1083/jcb.4.1.119

802 Toloue, M., Risinger, J., & Nakashe, P. (2013). Molecular Indexing for Improved RNA-Seq
803 Analysis. *Journal of Molecular Diagnostics*, 15(6), 939-939. Retrieved from <Go to
804 ISI>://WOS:000326668000374

805 Vogel, H., Grieninger, G. E., & Zetsche, K. H. (2002). Differential messenger RNA gradients in
806 the unicellular alga *Acetabularia acetabulum*. Role of the cytoskeleton. *Plant*
807 *Physiology*, 129(3), 1407-1416. doi:10.1104/pp.010983

808 Vugrek, O., Sawitzky, H., & Menzel, D. (2003). Class XIII myosins from the green alga
809 *Acetabularia*: driving force in organelle transport and tip growth? *J Muscle Res Cell*
810 *Motil*, 24(1), 87-97. doi:10.1023/a:1024898520419

811 Werz, G. (1955). Kernphysiologische Untersuchungen an *Acetabularia*. *Planta*, 46(2), 113-
812 153. doi:Doi 10.1007/Bf01963403

813 Wickens, M. (1992). Forward, backward, how much, when: mechanisms of poly(A) addition
814 and removal and their role in development. *Semin. Dev. Biol.*, 3, 399-412.

815 Wickham, H. (2016). *ggplot2: Elegant Graphics for Data Analysis*: Springer-Verlag New York.

816 Yasinovski, V. G., Zubarev, T. N., Rogatykh, N. P., & Yanushevich, I. V. (1979). Kinetics of
817 synthesis and distribution of the morphogenetic substances in whole cells and in
818 anucleate fragments of *Acetabularia mediterranea*. In S. Bonotto, V. Kefeli, & S.
819 Puisseux-Dao (Eds.), *Developmental biology of Acetabularia* (Vol. 3, pp. 65-70).
820 Amsterdam, Holland
821 New York, NY
822 Oxford, England: Elsevier/North_Holland Biomedical Press.

823 Young, M. D., Wakefield, M. J., Smyth, G. K., & Oshlack, A. (2010). Gene ontology analysis for
824 RNA-seq: accounting for selection bias. *Genome Biology*, 11(2). doi:ARTN R14
825 10.1186/gb-2010-11-2-r14
826
827
828

829 Supplementary information

830 Supplementary tables

831
832 **Table S1.** Chloroplast genomes used as BLAST database to identify *Acetabularia acetabulum*
833 chloroplast transcripts.

Organism	Size (bp)	Accession
Bacillariophyta;Coccosinodiscophyceae;Coccosinodisciales;Coccosinodiscaceae;Coccosinodiscus radiatus	122213	NC_024081
Bacillariophyta;Coccosinodiscophyceae;Rhizosoleniales;Rhizosoleniaceae;Rhizosolenia imbricata	120956	NC_025311
Bacillariophyta;Mediophyceae;Chaetocerotales;Chaetocerotaceae;Chaetoceros simplex	116459	NC_025310
Bacillariophyta;Mediophyceae;Hemiaulales;Hemiaulaceae;Cerataulina daemon	120144	NC_025313
Bacillariophyta;Mediophyceae;Lithodesmiales;Lithodesmiaceae;Lithodesmium undulatum	122660	NC_024085
Bacillariophyta;Mediophyceae;Thalassiosirales;Thalassiosiraceae;Roundia cardiophora	126871	NC_025312
Bacillariophyta;Fragilariophyceae;Fragilariales;Fragilariaceae;Asterionellopsis glacialis	146024	NC_024080
Chlorophyta;Chlorophyceae;Chlamydomonadales;Chlamydomonadales incertae sedis;Ettlia pseudoalveolaris	145947	NC_025332
Chlorophyta;Chlorophyceae;Oedogoniales;Oedogoniaceae;Oedocladium carolinianum	204438	NC_031510
Chlorophyta;Chlorophyceae;Sphaeropleales;Bracteacoccaceae;Bracteacoccus minor	192761	NC_029674
Chlorophyta;Chlorophyceae;Sphaeropleales;Bracteacoccaceae;Bracteacoccus aerius	165732	NC_029675
Chlorophyta;Chlorophyceae;Sphaeropleales;Bracteacoccaceae;Bracteacoccus giganteus	242897	NC_028586
Chlorophyta;Chlorophyceae;Sphaeropleales;Chromochloridaceae;Chromochloris zofingiensis	188935	NC_029672
Chlorophyta;Chlorophyceae;Sphaeropleales;Neochloridaceae;Neochloris aquatica	166767	NC_029670
Chlorophyta;Chlorophyceae;Sphaeropleales;Scenedesmaceae;Acutodesmus obliquus	161452	NC_008101
Chlorophyta;Pedinophyceae;Pedinomonadales;Pedinomonadaceae;Pedinomonas tuberculata	126694	NC_025330
Chlorophyta;Trebouxiophyceae;Chlorellales;Chlorellaceae;Auxenochlorella protothecoides	84576	NC_023775
Chlorophyta;Trebouxiophyceae;Chlorellales;Chlorellaceae;Pabia signiensis	236463	NC_025329
Chlorophyta;Trebouxiophyceae;Microthamniales;;Stichococcus bacillaris	116952	NC_025327
Chlorophyta;Trebouxiophyceae;Microthamniales;;Elliptochloris bilobata	134677	NC_025348
Chlorophyta;Trebouxiophyceae;Microthamniales;Microthamniaceae;Fusochloris perforata	148459	NC_025343
Chlorophyta;Trebouxiophyceae;Microthamniales;Microthamniaceae;Microthamnion kuetzingianum	158609	NC_025337
Chlorophyta;Trebouxiophyceae;Prasiolales;Koliellaceae;Koliella longiseta	197094	NC_025331
Chlorophyta;Trebouxiophyceae;Prasiolales;Prasiolaceae;Chlorella mirabilis	167972	NC_025328

Chlorophyta;Trebouxiophyceae;Trebouxiophyceae incertae sedis;Coccomyxaceae;Choricystis parasitica	94206	NC_025539
Chlorophyta;Trebouxiophyceae;Trebouxiophyceae incertae sedis;Coccomyxaceae;Paradoxia multisetata	183394	NC_025540
Chlorophyta;Trebouxiophyceae;Trebouxiales;Botryococcaceae;Botryococcus braunii	172826	NC_025545
Chlorophyta;Trebouxiophyceae;Trebouxiales;Trebouxiaceae;Myrmecia israelensis	146596	NC_025525
Chlorophyta;Ulvophyceae;Bryopsidales;Caulerpaceae;Caulerpa cliftonii	131135	NC_031368
Chlorophyta;Ulvophyceae;Bryopsidales;Caulerpaceae;Caulerpa racemosa	176522	NC_032042
Chlorophyta;Ulvophyceae;Bryopsidales;Codiaceae;Codium simulans	91509	NC_032043
Chlorophyta;Ulvophyceae;Ignatiales;Ignatiaceae;Ignatius tetrasporus	239387	NC_034712
Chlorophyta;Ulvophyceae;Ignatiales;Ignatiaceae;Pseudocharacium americanum	239448	NC_034711
Chlorophyta;Ulvophyceae;Oltmannsiellopsidales;Oltmannsiellopsidaceae;Neodangemania microcystis	166355	NC_034713
Chlorophyta;Ulvophyceae;Ulotrichales;Hazeniaceae;Hazenaria capsulata	189599	NC_034714
Chlorophyta;Ulvophyceae;Ulotrichales;Ulotrichaceae;Gloeotilopsis sterilis	132626	NC_025538
Chlorophyta;Ulvophyceae;Ulotrichales;Ulotrichales familia incertae sedis;Trichosarcina mucosa	227181	NC_034709
Chlorophyta;Ulvophyceae;Ulvaes;Ulvaceae;Pseudoneochloris marina	134753	NC_034710
Chlorophyta;Ulvophyceae;Ulvaes;Ulvaceae;Ulva fasciata	96005	NC_029040
Chlorophyta;Ulvophyceae;Ulvaes;Ulvaceae;Ulva linza	86726	NC_030312
Chlorophyta;Ulvophyceae;Ulvaes;Ulvaceae;Ulva flexuosa	89414	NC_035823
Chlorophyta;Ulvophyceae;Ulvaes;Ulvaceae;Ulva prolifera	93066	NC_036137
Charophyta;Zygnemophyceae;Zygnematales;Mesotaeniaceae;Roya anglica	138275	NC_024168
Charophyta;Zygnemophyceae;Zygnematales;Mesotaeniaceae;Mesotaenium endlicherianum	142017	NC_024169
Euglenozoa;Euglenophyceae;Euglenales;Euglenaceae;Monomorphina parapyrum	80147	NC_027287
Euglenozoa;Euglenophyceae;Euglenales;Euglenaceae;Trachelomonas volvocina	85392	NC_027288
Euglenozoa;Euglenophyceae;Euglenales;Euglenaceae;Euglenaria anabaena	88487	NC_027269
Haptophyta;Coccolithophyceae;Phaeocystales;Phaeocystaceae;Phaeocystis antarctica	105512	NC_016703
Haptophyta;Coccolithophyceae;Phaeocystales;Phaeocystaceae;Phaeocystis globosa	107461	NC_021637
Ochrophyta;Eustigmatophyceae;Eustigmatales;Monodopsidaceae;Nannochloropsis granulata	117672	NC_022259
Ochrophyta;Phaeophyceae;Laminariales;Laminariaceae;Saccharina japonica	130584	NC_018523
Rhodophyta;Bangiophyceae;Bangiales;Bangiaceae;Pyropia perforata	189789	NC_024050
Rhodophyta;Compsopogonophyceae;Compsopogonales;Boldiaceae;Boldia erythrosiphon	226658	NC_034776
Rhodophyta;Florideophyceae;Gracilariales;Gracilariaceae;Gracilaria salicornia	179757	NC_023785

Rhodophyta;Porphyridiophyceae;Porphyridiales;Porphyridiaceae;Porphyridium purpureum	217694	NC_023133
Streptophyta;Zygnemophyceae;Desmidiales;Desmidiaceae;Cosmarium botrytis	207850	NC_030357
Streptophyta;Zygnemophyceae;Zygnematales;Zygnemataceae ;Entransia fimbriata	206025	NC_030313
Streptophyta;Zygnemophyceae;Zygnematales;Zygnemataceae ;Spirogyra maxima	129954	NC_030355
Streptophyta;Zygnemophyceae;Zygnematales;Zygnemataceae ;Netrium digitus	131804	NC_030356

834

835 **Table S2.** Mitochondrial genomes used as BLAST database to identify *Acetabularia acetabulum*
 836 mitochondrial transcripts

Organism	Size (bp)	Accession
Eukaryota;Stramenopiles;PX clade;Phaeophyceae;Laminariales;Laminariaceae;Saccharina;Saccharina latissima	3765 9	NC_02 6108
Eukaryota;Sar;Stramenopiles;Ochrophyta;PX clade;Phaeophyceae;Laminariales;Laminariaceae;Saccharina;Saccharina japonica	3765 7	NC_01 3476
Eukaryota;Stramenopiles;Eustigmatophyceae;Eustigmatales;Monodopsidaceae;Nannochloropsis;Nannochloropsis oceanica	3805 7	NC_02 2258
Eukaryota;Rhodophyta;Florideophyceae;Rhodymeniophycidae;Gracilariales;Gracilariaceae;Gracilaria;Gracilaria salicornia	2527 2	NC_02 3784
Eukaryota;Viridiplantae;Streptophyta;Zygnemophyceae;Zygnematales;Mesotaeniaceae;Roya;Roya obtusa	6946 5	NC_02 2863
Eukaryota;Rhodophyta;Bangiophyceae;Bangiales;Bangiaceae;Pyropia;Pyropia nitida	3531 3	NC_02 7616
Eukaryota;Viridiplantae;Chlorophyta;Trebouxiophyceae;Trebouxiophyceae incertae sedis;Botryococcaceae;Botryococcus;Botryococcus braunii	8458 3	NC_02 7722
Eukaryota;Viridiplantae;Chlorophyta;Trebouxiophyceae;Chlorellales;Chlorellaceae;Chlorella	5252 8	NC_02 4626
Eukaryota;Viridiplantae;Chlorophyta;Trebouxiophyceae;Chlorellales;Chlorellaceae;Auxenochlorella;Auxenochlorella protothecoides	5727 4	NC_02 6009
Eukaryota;Viridiplantae;Chlorophyta;core chlorophytes;Trebouxiophyceae;Chlorellales;Chlorellaceae;Chlorella clade;Chlorella;Chlorella variabilis	7850 0	NC_02 5413
Eukaryota;Viridiplantae;Chlorophyta;Pedinophyceae;Pedinomonadales;Pedinomonadaceae;Pedinomonas;Pedinomonas minor	2513 7	NC_00 0892
Eukaryota;Viridiplantae;Chlorophyta;Chlorophyceae;Sphaeropleales;Neochloridaceae;Neochloris;Neochloris aquatica	3802 1	NC_02 4761
Eukaryota;Viridiplantae;Chlorophyta;Chlorophyceae;Sphaeropleales;Chromochloridaceae;Chromochloris;Chromochloris zofingiensis	4484 0	NC_02 4758
Eukaryota;Viridiplantae;Chlorophyta;Chlorophyceae;Sphaeropleales;Neochloridaceae;Chlorotetraedron;Chlorotetraedron incus	3840 6	NC_02 4757
Eukaryota;Viridiplantae;Chlorophyta;Chlorophyceae;Sphaeropleales;Bracteacoccaceae;Bracteacoccus;Bracteacoccus aerius	4715 8	NC_02 4755
Eukaryota;Viridiplantae;Chlorophyta;Chlorophyceae;Sphaeropleales;Bracteacoccaceae;Bracteacoccus;Bracteacoccus minor	4517 5	NC_02 4756
Eukaryota;Viridiplantae;Streptophyta;Zygnemophyceae;Zygnematales;Zygnemataceae;Entransia;Entransia fimbriata	6164 5	NC_02 2861
Eukaryota;Viridiplantae;Chlorophyta;Ulvophyceae;OUU clade;Ulvaes;Ulvaceae;Ulva;Ulva fasciata	6161 4	NC_02 8081
Eukaryota;Viridiplantae;Chlorophyta;Ulvophyceae;OUU clade;Ulvaes;Ulvaceae;Ulva;Ulva prolifera	6384 5	NC_02 8538
Eukaryota;Viridiplantae;Chlorophyta;Ulvophyceae;OUU clade;Ulvaes;Ulvaceae;Ulva;Ulva linza	7085 8	NC_02 9701
Eukaryota;Viridiplantae;Chlorophyta;Ulvophyceae;OUU clade;Ulvaes;Ulvaceae;Ulva;Ulva pertusa	6933 3	NC_03 5722
Eukaryota;Viridiplantae;Chlorophyta;Ulvophyceae;OUU clade;Ulvaes;Ulvaceae;Ulva;Ulva flexuosa	7154 5	NC_03 5809
Eukaryota;Viridiplantae;Chlorophyta;Chlorophyceae;Sphaeropleales;Selenastraceae;Ourococcus;Ourococcus multisporus	4970 5	NC_02 4762
Eukaryota;Viridiplantae;Chlorophyta;Chlorophyceae;Chlamydomonadales;Chlamydomonadaeae;Polytoma;Polytoma uvella	1741 1	NC_02 6572

837

838 **Table S3.** rRNA sequences from various green algae used as BLAST database to identify
839 *Acetabularia* rRNA transcripts.

Organism	Gene	Size (bp)	Accession
Eukaryota;Viridiplantae;Chlorophyta;Ulvophyceae;Ignatiales;Ignatius;Ignatius tetrasporus	18S (partial)	1744	AB110439
Eukaryota;Viridiplantae;Chlorophyta;Ulvophyceae;Ignatiales;Pseudocharacium;Pseudocharacium americanum	18S (partial)	1743	AB110440
Eukaryota;Viridiplantae;Chlorophyta;Ulvophyceae;Oltmannsiellopsidales;Oltmannsiellopsidaceae;Oltmannsiellopsis;Oltmannsiellopsis geminata	18S (partial)	1745	AB183610
Eukaryota;Viridiplantae;Chlorophyta;Ulvophyceae;TCBD clade;Dasycladales;Polyphysaceae;Acetabularia;Acetabularia acetabulum	18S (partial)	1042	AF493616
Eukaryota;Viridiplantae;Chlorophyta;Ulvophyceae;OUU clade;Ulvaes;Ulvaceae;Blidingia;Blidingia minima	5.8S	615	AJ000206
Eukaryota;Viridiplantae;Chlorophyta;Ulvophyceae;OUU clade;Ulvaes;Ulvaceae;Blidingia;Blidingia chadefaudii	5.8S	569	AJ012309
Eukaryota;Viridiplantae;Chlorophyta;Ulvophyceae;TCBD clade;Bryopsidales;Caulerpaceae;Caulerpa;Caulerpa taxifolia	18S, 28S and 5.8S	641	AJ299742
Eukaryota;Viridiplantae;Chlorophyta;Ulvophyceae;TCBD clade;Dasycladales;Polyphysaceae;Acetabularia;Acetabularia acetabulum	18S	1773	AY165775
Eukaryota;Viridiplantae;Chlorophyta;Ulvophyceae;Ulvophyceae;incertae sedis;Oltmannsiellopsis;Oltmannsiellopsis viridis	18S	1746	D86495
Eukaryota;Viridiplantae;Chlorophyta;core chlorophytes;Trebouxiophyceae;Chlorellales;Chlorellaceae;Chlorella clade;Actinastrum;Actinastrum hantzschii	18S (partial), 5.8S and 28S (partial)	2874	FM205841
Eukaryota;Viridiplantae;Chlorophyta;core chlorophytes;Trebouxiophyceae;Chlorellales;Chlorellaceae;Chlorella clade;Chlorella;Chlorella heliozoae	18S (partial), 5.8S and 28S (partial)	3852	FM205850
Eukaryota;Viridiplantae;Chlorophyta;core chlorophytes;Trebouxiophyceae;Chlorellales;Chlorellaceae;Chlorella clade;Actinastrum;Actinastrum hantzschii	18S (partial), 5.8S and 28S (partial)	3113	FM205882
Eukaryota;Viridiplantae;Chlorophyta;core chlorophytes;Trebouxiophyceae;Chlorellales;Chlorellaceae;Chlorella clade;Actinastrum;Actinastrum hantzschii	18S (partial), 5.8S and 28S (partial)	2530	FM205884
Eukaryota;Viridiplantae;Chlorophyta;Ulvophyceae;OUU clade;Ulotrichales;Chlorocystidaceae;Desmochloris;Desmochloris halophila	18S (partial) and 5.8S	2347	FM882216
Eukaryota;Viridiplantae;Chlorophyta;Ulvophyceae;OUU clade;Ulotrichales;Chlorocystidaceae;Desmochloris;Desmochloris mollenhaueri	18S (partial) and 5.8S	2777	FM882217
Eukaryota;Viridiplantae;Chlorophyta;Ulvophyceae;TCBD clade;Trentepohliales;Trentepohliaceae;Trentepohlia;unclassified Trentepohlia;Trentepohlia sp. CB-2010	28S (partial)	549	FR719952
Eukaryota;Viridiplantae;Chlorophyta;Ulvophyceae;Oltmannsiellopsidales;Oltmannsiellopsidaceae;Oltmannsiellopsis;unclassified Oltmannsiellopsis;Oltmannsiellopsis sp. CCMP1240	18S (partial), 5.8S and 28S (partial)	5585	HE610120
Eukaryota;Viridiplantae;Chlorophyta;Ulvophyceae;Ignatiales;Ignatiaceae;Ignatius;Ignatius tetrasporus	18S (partial), 5.8S and 28S (partial)	3790	HE610121
Eukaryota;Viridiplantae;Chlorophyta;Ulvophyceae;OUU clade;Ulotrichales;Ulotrichaceae;Ulothrix;Ulothrix zonata	28S (partial)	583	HE860527
Eukaryota;Viridiplantae;Chlorophyta;Ulvophyceae;OUU clade;Ulvaes;Ulvaceae;Blidingia;Blidingia marginata	28S (partial)	603	HQ603266
Eukaryota;Viridiplantae;Chlorophyta;Ulvophyceae;Ulvophyceae;incertae sedis;Smithsoniella;Smithsoniella earleae	18S (partial)	1738	JF680958
Eukaryota;Viridiplantae;Chlorophyta;core chlorophytes;Trebouxiophyceae;Chlorellales;Chlorellaceae;Chlorella clade;Chlorella;Chlorella sorokiniana	18S, 5.8S and 28S (partial)	2527	LK021940
Eukaryota;Viridiplantae;Chlorophyta;Ulvophyceae;TCBD clade;Dasycladales;Polyphysaceae;Acetabularia;Acetabularia caliculus	18S (partial)	520	MF579955
Eukaryota;Viridiplantae;Chlorophyta;Ulvophyceae;TCBD clade;Dasycladales;Polyphysaceae;Acetabularia;Acetabularia acetabulum	18S	1766	Z33461

840

841 **Table S4.** *Chlamydomonas reinhardtii* COP and Clathrin genes used to identify similar genes in *A.*
842 *acetabulum*

Gene	Accession number
alpha-COP	XP_001693686
beta-COP	XP_001701255
beta-COP	XP_001702422
delta-COP	XP_001701763
epsilon-COP	XP_001693085
gamma-COP	XP_001691193
zeta-COP, subunit of COP-1 complex	XP_001701294
sar-type small GTPase	XP_001699537
COP-II coat subunit	XP_001700438
COP-II coat subunit	XP_001702936
COP-II coat subunit	XP_001701974
COP-II coat subunit	XP_001697039
Clathrin heavy chain	XP_001699806

843

844

845 **Table S5. RNA isolation.**

	Single Cell RNA purification Kit	Total RNA purification kit	% Increase by using the Total RNA purification kit
Mean total RNA yield (ng)	33	159	382
Mean transcripts with count > 0	51715	55031	6
Mean transcripts with count > 1	35019	37170	6
Mean transcripts with count > 2	28821	30510	6
Mean transcripts with count > 3	25474	26897	6

846

847 **Table S6.** Assembly statistics of the *de novo* assembled transcriptome of *Acetabularia acetabulum*.
848 Only the highest expressed isoform of each gene is represented in the transcriptome. This transcriptome
849 was used as a mapping reference for further RNA-seq analysis.

<i>A. acetabulum</i> transcriptome	
Total transcriptome size (bp)	114 907 754
Number of transcripts	246 083
Longest transcript (bp)	17 196
Shortest transcript (bp)	201
Mean transcript length (bp)	467
Median transcript length (bp)	298
N50 transcript length (bp)	534

Nuclear encoded transcripts	245 334
mRNAs	245 223
rRNAs	111
Chloroplast encoded transcripts	389
Mitochondrial encoded transcripts	99
Possible prokaryotic/unclassified transcripts	261

Predicted protein coding transcripts (TransDecoder)	114 146
Nuclear	113 900
Chloroplast	178
Mitochondrial	68

850

851 **Table S7. Enriched Gene Ontologies.** Domain refers to “Cellular Component” (CC), “Biological
 852 Process” (BP) and “Molecular Function” (MF). FDR refers to the False Discovery Rates calculated on
 853 the p-values by the qvalue function in the R package qvalue. The “%” in the Cap, Stalk and Rhizoid is
 854 the percentage of GO-ID’s in the enriched pool of transcripts (in the Cap, Stalk or Rhizoid) compared
 855 to the number in the total transcriptome.

ID	Term	Domain	Cap FDR	Cap %	Stalk FDR	Stalk %	Rhizoid FDR	Rhizoid %
GO:0005623	cell	CC	4.3E-181	20	4.9E-34	5	1.1E-208	23.2
GO:0009536	plastid	CC	2.2E-103	35	3.3E-04	4	1.5E-02	8.1
GO:0009579	thylakoid	CC	1.8E-60	47	0	0	0	0
GO:0006950	response to stress	BP	1.0E-40	23	3.8E-06	5	8.3E-30	22
GO:0009058	biosynthetic process	BP	1.5E-37	23	4.6E-07	6	1.3E-32	23
GO:0005829	cytosol	CC	2.7E-31	19	6.0E-06	4	1.3E-47	24
GO:0043167	ion binding	MF	5.3E-28	26	0	0	6.4E-17	22
GO:0005886	plasma membrane	CC	2.5E-25	22	6.3E-03	4	1.1E-24	24
GO:0022857	transmembrane transporter activity	MF	2.5E-25	40	4.0E-03	7	9.9E-03	12
GO:0044281	small molecule metabolic process	BP	5.4E-25	29	2.8E-05	7	5.0E-10	20
GO:0016491	oxidoreductase activity	MF	5.7E-23	34	0	0	2.3E-03	13
GO:0005773	vacuole	CC	3.7E-21	27	2.4E-03	5	1.3E-05	15
GO:0051186	cofactor metabolic process	BP	2.0E-20	34	1.1E-02	6	7.7E-04	14
GO:0015979	photosynthesis	BP	8.1E-20	38	0	0	0	0
GO:0005739	mitochondrion	CC	9.3E-20	24	2.1E-02	4	4.0E-11	20
GO:0032991	protein-containing complex	CC	8.8E-18	14	3.7E-07	5	3.9E-86	29
GO:0065003	protein-containing complex assembly	BP	2.3E-17	26	0	0	2.1E-22	31
GO:0006091	generation of precursor metabolites and energy	BP	3.8E-17	29	0	0	3.2E-03	11
GO:0042592	homeostatic process	BP	1.9E-16	28	0	0	2.2E-08	21
GO:0006520	cellular amino acid metabolic process	BP	6.0E-16	36	0	0	3.4E-05	20
GO:0005576	extracellular region	CC	1.0E-15	31	2.0E-02	6	1.0E-03	14
GO:0006629	lipid metabolic process	BP	1.2E-15	29	6.7E-03	6	1.0E-05	19
GO:0005794	Golgi apparatus	CC	1.4E-15	26	5.2E-03	6	1.6E-05	17
GO:0016887	ATPase activity	MF	4.2E-15	34	0	0	1.8E-03	16
GO:0019899	enzyme binding	MF	6.7E-15	27	8.4E-04	7	1.8E-08	21
GO:0005783	endoplasmic reticulum	CC	2.8E-13	24	0	0	1.3E-13	26
GO:0005840	ribosome	CC	2.5E-12	15	0	0	4.2E-18	21
GO:0006790	sulfur compound metabolic process	BP	3.0E-12	38	0	0	4.3E-03	16
GO:0009056	catabolic process	BP	4.0E-12	23	3.8E-06	9	1.1E-06	18
GO:0007165	signal transduction	BP	1.1E-11	18	7.7E-05	6	9.1E-21	26
GO:0003735	structural constituent of ribosome	MF	3.7E-11	15	0	0	7.5E-14	18
GO:0000003	reproduction	BP	3.9E-11	18	9.6E-04	5	7.4E-22	26
GO:0034641	cellular nitrogen compound metabolic process	BP	4.6E-11	17	3.4E-03	4	1.7E-22	24
GO:0061024	membrane organization	BP	1.6E-10	27	4.7E-02	5	2.7E-08	24

GO:0006605	protein targeting	BP	1.6E-10	24	0	0	5.4E-07	20
GO:0016192	vesicle-mediated transport	BP	1.8E-10	22	4.0E-06	9	3.6E-10	23
GO:0048856	anatomical structure development	BP	1.9E-10	17	4.7E-08	8	5.0E-18	23
GO:0006412	translation	BP	1.1E-09	15	2.2E-02	3	2.1E-20	24
GO:0007568	aging	BP	1.6E-09	33	0	0	8.3E-05	22
GO:0005618	cell wall	CC	8.4E-09	22	0	0	2.6E-05	17
GO:0048646	anatomical structure formation involved in morphogenesis	BP	9.4E-09	24	0	0	9.0E-06	20
GO:0009790	embryo development	BP	1.3E-08	23	0	0	2.3E-09	25
GO:0002376	immune system process	BP	2.1E-08	20	3.2E-02	5	2.3E-13	28
GO:0016829	lyase activity	MF	4.5E-08	32	0	0	9.3E-04	19
GO:0006810	transport	BP	4.5E-08	35	0	0	9.6E-05	25
GO:0006464	cellular protein modification process	BP	6.4E-08	15	9.6E-04	5	4.0E-31	29
GO:0030154	cell differentiation	BP	8.7E-08	17	5.4E-03	5	1.0E-20	29
GO:0008219	cell death	BP	1.4E-07	21	8.4E-03	7	4.0E-09	25
GO:0003013	circulatory system process	BP	1.7E-07	60	0	0	0	0
GO:0034655	nucleobase-containing compound catabolic process	BP	3.4E-07	18	1.2E-02	5	1.5E-09	23
GO:0007267	cell-cell signaling	BP	4.4E-07	30	5.2E-03	11	2.3E-07	32
GO:0005764	lysosome	CC	4.7E-07	29	5.2E-03	10	8.8E-03	15
GO:0005975	carbohydrate metabolic process	BP	4.9E-07	20	3.8E-06	11	1.5E-04	17
GO:0031410	cytoplasmic vesicle	CC	6.2E-07	27	1.2E-03	11	3.1E-04	20
GO:0005768	endosome	CC	1.4E-06	20	7.1E-03	7	1.9E-09	25
GO:0005634	nucleus	CC	1.8E-06	14	8.7E-04	5	3.3E-33	30
GO:0055085	transmembrane transport	BP	2.6E-06	26	0	0	1.1E-03	19
GO:0016301	kinase activity	MF	3.4E-06	20	0	0	4.5E-07	23
GO:0015031	protein transport	BP	5.8E-06	18	4.0E-03	7	9.1E-17	33
GO:0007010	cytoskeleton organization	BP	1.0E-05	18	0	0	4.6E-28	43
GO:0005856	cytoskeleton	CC	1.1E-05	18	0	0	1.3E-20	39
GO:0021700	developmental maturation	BP	1.4E-05	33	0	0	1.5E-02	17
GO:0042254	ribosome biogenesis	BP	1.8E-05	12	0	0	1.0E-16	24
GO:0008092	cytoskeletal protein binding	MF	2.0E-05	20	0	0	2.5E-13	36
GO:0019748	secondary metabolic process	BP	2.4E-05	36	0	0	1.3E-02	18
GO:0007034	vacuolar transport	BP	2.9E-05	27	3.2E-02	9	1.3E-02	16
GO:0051604	protein maturation	BP	2.9E-05	29	0	0	2.9E-03	20
GO:0008233	peptidase activity	MF	2.9E-05	20	1.2E-03	9	1.5E-03	16
GO:0016874	ligase activity	MF	4.4E-05	24	0	0	2.4E-05	26
GO:0050877	nervous system process	BP	4.6E-05	29	0	0	2.5E-06	35
GO:0051301	cell division	BP	4.7E-05	19	2.8E-02	6	2.7E-14	36
GO:0000902	cell morphogenesis	BP	5.2E-05	18	0	0	1.0E-13	32
GO:0003723	RNA binding	MF	7.4E-05	15	3.1E-05	9	4.7E-10	24
GO:0003729	mRNA binding	MF	8.5E-05	13	0	0	9.0E-07	17
GO:0005730	nucleolus	CC	1.2E-04	12	0	0	1.3E-12	22
GO:0040007	growth	BP	1.5E-04	15	0	0	1.7E-14	29

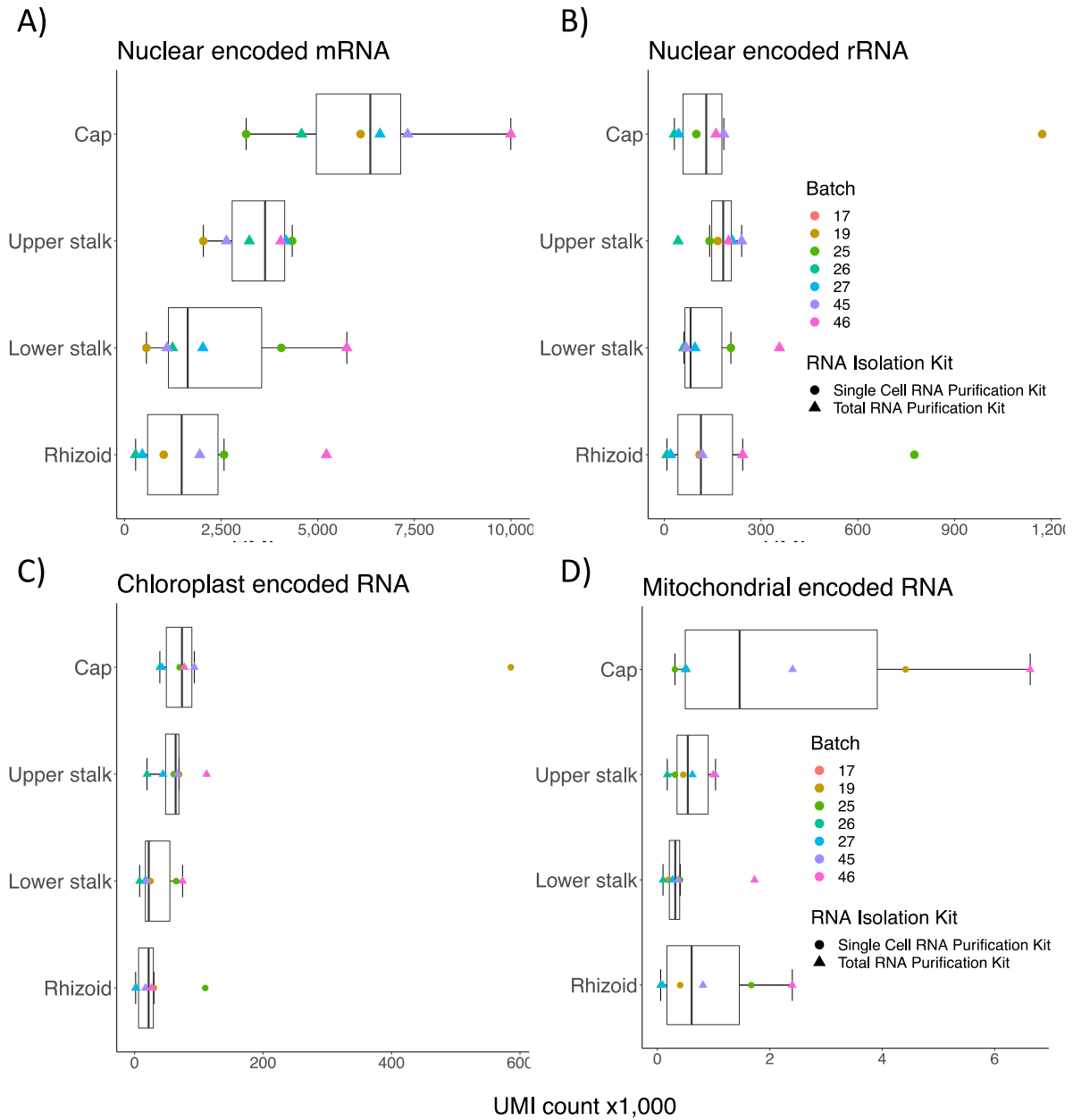
GO:0016853	isomerase activity	MF	1.7E-04	22	0	0	3.9E-09	37
GO:0007005	mitochondrion organization	BP	1.7E-04	22	0	0	2.6E-05	25
GO:0006914	autophagy	BP	2.1E-04	21	0	0	2.0E-05	26
GO:0005929	cilium	CC	4.3E-04	22	0	0	4.0E-18	59
GO:0005777	peroxisome	CC	5.0E-04	24	1.1E-02	12	7.4E-03	18
GO:0030234	enzyme regulator activity	MF	5.1E-04	16	3.4E-03	9	1.4E-11	34
GO:0005815	microtubule organizing center	CC	5.1E-04	22	0	0	4.9E-09	42
GO:0016791	phosphatase activity	MF	5.5E-04	19	3.1E-04	13	6.0E-03	16
GO:0019843	rRNA binding	MF	6.8E-04	16	0	0	2.5E-06	25
GO:0044403	symbiont process	BP	7.2E-04	20	0	0	5.8E-07	32
GO:0030198	extracellular matrix organization	BP	7.4E-04	30	0	0	1.3E-02	20
GO:0007155	cell adhesion	BP	7.7E-04	22	0	0	8.1E-07	37
GO:0006913	nucleocytoplasmic transport	BP	8.0E-04	16	0	0	4.3E-09	31
GO:0022607	cellular component assembly	BP	8.4E-04	15	1.8E-02	7	5.5E-09	27
GO:0005615	extracellular space	CC	9.3E-04	18	1.2E-03	12	2.1E-02	12
GO:0016757	transferase activity, transferring glycosyl groups	MF	1.1E-03	24	0	0	3.2E-02	14
GO:0006457	protein folding	BP	1.2E-03	20	0	0	4.2E-06	31
GO:0016765	transferase activity, transferring alkyl or aryl (other than methyl) groups	MF	1.2E-03	26	0	0	2.1E-02	16
GO:0071554	cell wall organization or biogenesis	BP	1.4E-03	19	3.8E-06	19	0	0
GO:0008289	lipid binding	MF	1.9E-03	18	0	0	3.7E-04	22
GO:0030705	cytoskeleton-dependent intracellular transport	BP	2.3E-03	29	0	0	5.5E-06	50
GO:0005198	structural molecule activity	MF	2.3E-03	24	0	0	1.9E-04	32
GO:0005635	nuclear envelope	CC	3.2E-03	19	0	0	1.2E-08	40
GO:0003677	DNA binding	MF	5.7E-03	12	3.2E-02	6	2.3E-19	38
GO:0006399	tRNA metabolic process	BP	6.3E-03	15	0	0	5.9E-10	36
GO:0022618	ribonucleoprotein complex assembly	BP	6.9E-03	9	0	0	2.4E-09	24
GO:0008283	cell proliferation	BP	6.9E-03	13	5.0E-03	8	2.0E-11	34
GO:0005622	intracellular	CC	7.4E-03	21	0	0	1.1E-06	47
GO:0003700	DNA-binding transcription factor activity	MF	7.4E-03	17	0	0	3.3E-03	20
GO:0140014	mitotic nuclear division	BP	7.8E-03	20	0	0	7.9E-04	28
GO:0008135	translation factor activity, RNA binding	MF	8.0E-03	19	4.5E-02	13	2.5E-04	31
GO:0007049	cell cycle	BP	8.1E-03	14	0	0	4.6E-12	39
GO:0071941	nitrogen cycle metabolic process	BP	8.5E-03	40	0	0	4.5E-02	20
GO:0007009	plasma membrane organization	BP	8.9E-03	50	0	0	4.7E-02	25
GO:0048870	cell motility	BP	1.0E-02	13	0	0	1.3E-20	49
GO:0005737	cytoplasm	CC	1.5E-02	10	8.7E-04	6	4.7E-39	37
GO:0000278	mitotic cell cycle	BP	1.5E-02	11	2.4E-03	8	2.2E-19	40
GO:0043226	organelle	CC	2.1E-02	17	8.7E-04	22	2.2E-02	17
GO:0040011	locomotion	BP	2.5E-02	14	0	0	8.3E-10	57

GO:0016810	hydrolase activity, acting on carbon-nitrogen (but not peptide) bonds	MF	2.5E-02	18	0	0	0	0
GO:0016746	transferase activity, transferring acyl groups	MF	3.0E-02	14	1.8E-02	14	2.8E-07	48
GO:0006259	DNA metabolic process	BP	3.1E-02	9	0	0	4.6E-28	38
GO:0051082	unfolded protein binding	MF	3.5E-02	15	0	0	2.8E-04	38
GO:0005654	nucleoplasm	CC	3.6E-02	8	0	0	1.1E-38	38
GO:0003924	GTPase activity	MF	3.6E-02	11	0	0	2.9E-08	40
GO:0000229	cytoplasmic chromosome	CC	4.2E-02	33	6.3E-03	67	0	0
GO:0004518	nuclease activity	MF	4.5E-02	10	1.7E-02	9	7.4E-09	34
GO:0005811	lipid droplet	CC	4.5E-02	20	0	0	5.0E-04	60
GO:0032196	transposition	BP	4.9E-02	25	0	0	4.3E-02	25
GO:0031012	extracellular matrix	CC	5.0E-02	20	0	0	7.6E-03	40
GO:0016798	hydrolase activity, acting on glycosyl bonds	MF	0	0	4.9E-03	13	3.4E-02	13
GO:0051276	chromosome organization	BP	0	0	4.9E-02	5	6.5E-24	38
GO:0000228	nuclear chromosome	CC	0	0	0	0	7.8E-14	39
GO:0005694	chromosome	CC	0	0	0	0	1.6E-10	45
GO:0006397	mRNA processing	BP	0	0	0	0	2.2E-08	30
GO:0007059	chromosome segregation	BP	0	0	0	0	7.5E-08	38
GO:0008134	transcription factor binding	MF	0	0	0	0	1.3E-07	50
GO:0008168	methyltransferase activity	MF	0	0	0	0	2.3E-07	36
GO:0030674	protein binding, bridging	MF	0	0	0	0	9.6E-07	41
GO:0043473	pigmentation	BP	0	0	0	0	1.5E-06	71
GO:0004386	helicase activity	MF	0	0	0	0	9.0E-05	29
GO:0016779	nucleotidyltransferase activity	MF	0	0	0	0	1.9E-04	28
GO:0034330	cell junction organization	BP	0	0	0	0	8.5E-04	27
GO:0042393	histone binding	MF	0	0	0	0	4.3E-03	27

857

858 Supplementary figures

859



860

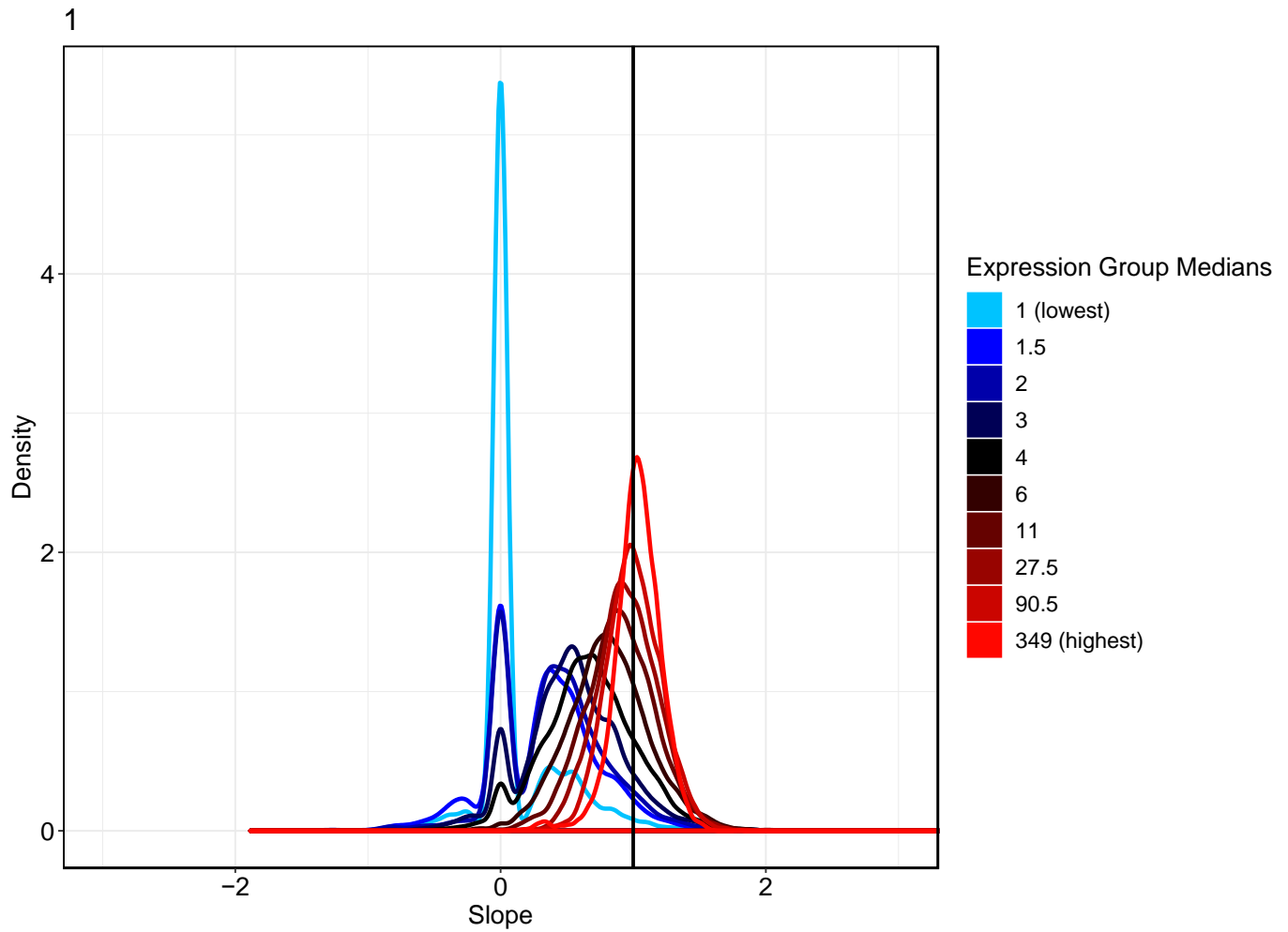
861 **Figure S1.** Boxplots showing the summarized gene expression levels (total UMI counts) of **A)** nuclear
862 encoded mRNA, **B)** nuclear encoded rRNA, **C)** chloroplast encoded RNA and **D)** mitochondrial
863 encoded RNA

864

865

866

867



868
869
870
871
872
873
874
875
876

Figure S2. Density plot generated with the `sc-norm` package in R, displaying the relationship between sequencing depth and gene counts in our samples. Genes are grouped into 10 groups based on gene expression (shown in colors). We see that for the highest expressed genes, the slope of the relationship between expression and sequencing depth is close to 1, justifying the use of normalization based on sequencing depth (as in the DESeq2 R package).

877
878
879
880
881
882